Chapter 2
Electrochemistry and Frontier Molecular Orbitals of Endohedral Metallofullerenes

Alexey A. Popov

Abstract Fullerenes exhibit rich redox activity and are able to accommodate up to 6 surplus electrons or give away 1–2 electrons in solution. EMFs inherit this property from empty fullerenes, and also add a new dimension to the redox behavior because endohedral clusters can exhibit their own redox activity despite their shielding by the carbon cage. This chapter provides a systematic overview of electrochemical properties of different classes of endohedral metallofullerenes. In particular, the balance between fullerene- and cluster-based redox activity in complex endohedral metallofullerenes is discussed using frontier molecular orbitals as a guide.

2.1 Introduction

Electrochemical properties of endohedral metallofullerenes (EMFs) were in focus of the research since mid-1990s, when the first isomerically pure samples became available [1–5]. Since that time, virtually any newly isolated EMF and many of their derivatives were characterized electrochemically, in particular by cyclic voltammetry or pulse voltammetric techniques (differential pulse voltammetry, DPV, and squarewave voltammetry, SWV). Redox potentials, especially those of the first oxidation and reduction steps ($E_{1/2}$(+/0) and $E_{1/2}$(0/−), hereafter), provide information on the electronic properties of fullerenes and enable straightforward estimation of the HOMO-LUMO gap. Electrochemical gap (gap_{EC}), defined as the difference between $E_{1/2}$(+/0) and $E_{1/2}$(0/−) values, can be used, along with the optical gap, as a measure of kinetic stability of fullerenes. Redox potentials discussed in this chapter are measured in *o*-dichlorobenzene and referred versus the $Fe(Cp)_2^{+/0}$ couple. We will not distinguish the values obtained by cyclic voltammetry (half-wave potentials, $E_{1/2}$, for reversible processes, and peak potentials for irre-

A.A. Popov (✉)
Leibniz Institute for Solid State and Materials Research,
Helmholtzstraße 20, 01069 Dresden, Germany
e-mail: a.popov@ifw-dresden.de

A.A. Popov (ed.), *Endohedral Fullerenes: Electron Transfer and Spin*,
Nanostructure Science and Technology, DOI 10.1007/978-3-319-47049-8_2

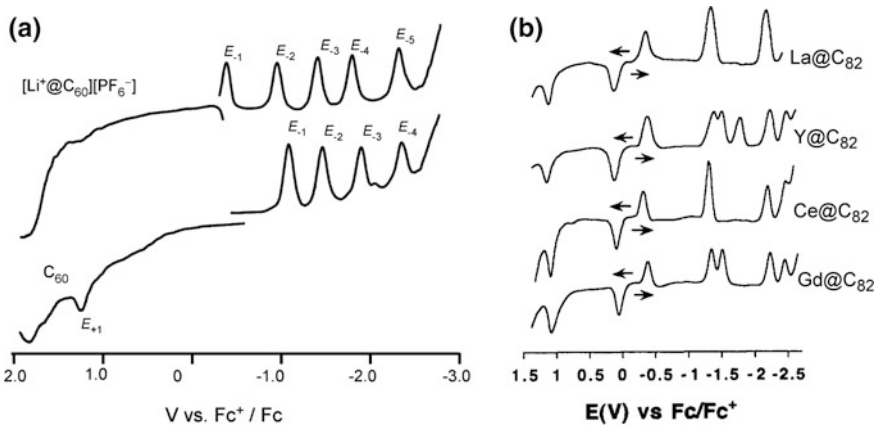

Fig. 2.1 **a** Squarewave voltammetry of the $[Li^+@C_{60}][PF_6^-]$ salt compared to that of fullerene C_{60}; Reproduced with permission from [16]. **b** Squarewave voltammetry of monometallofullerenes $M^{III}@C_{82}$-C_{2v}(9) with trivalent lanthanides measured in *o*-dichlorobenzene. Reproduced with permission from [3]

versible processes) and those determined by pulse method (SWV, DPV). Deviations between such values are usually less than few tens mV, which is not substantial for an overview of electrochemical properties of EMFs.

Fullerenes are known as good electron acceptors and undergo multiple electrochemically reversible single-electron redox processes in solution. Electrochemical studies of C_{60} showed that it is able to accept up to 6 electrons under optimized conditions at reduced temperature [6], whereas three–four reversible reductions steps are usually accessible at room temperature in *o*-dichlorobenzene (*o*-DCB, the most common solvent for electrochemical studies of fullerenes; Fig. 2.1). Similar cathodic behavior is exhibited by higher fullerenes [7–10]. Oxidation of C_{60} and C_{70} fullerenes occurs at relatively high potentials, making it difficult to achieve the reversible process in standard electrochemical studies [11–14]. However, oxidation of many other higher fullerenes (C_{76}, C_{78}, C_{82}, C_{84} etc.) occurs at less positive potentials and usually one or even two oxidation steps can be accessed [8, 9, 15].

Encapsulation of metal atoms and clusters in EMFs can result in more complex redox behavior than that of empty fullerenes. The carbon cage in the EMF molecule can be considered as a special type of π-ligand, similar to those in organometallic complexes (e.g., as in ferrocene). In terms of organometallic electrochemistry, the ligand can be "non-innocent," when it exhibits its own redox activity, or "innocent," when it does not take part in the redox process. In a similar fashion, both the fullerene cage and the endohedral species can exhibit redox activity in EMFs. Figure 2.2 shows two extremes of such redox behavior. In the first case, only the carbon cage is redox-active, meaning that the valence and spin state endohedral species remains intact during electrochemical processes (i.e., fullerene behaves as

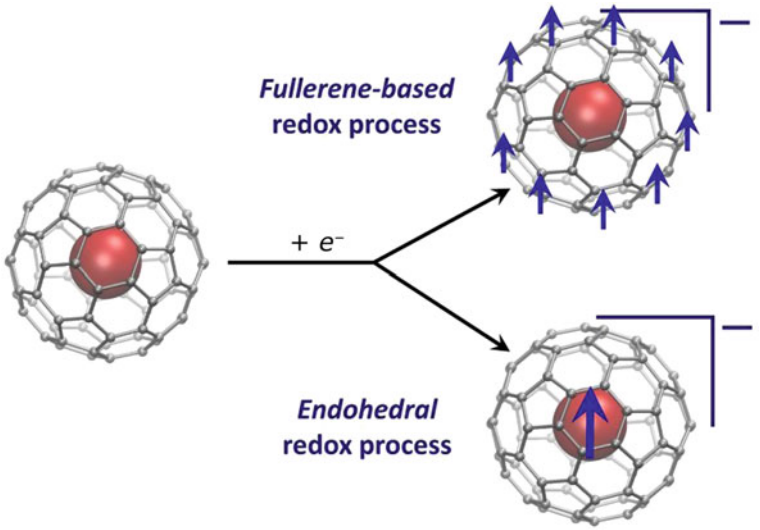

Fig. 2.2 Schematic description of the fullerene-based and endohedral redox processes. In the former, with the surplus charge and spin density are delocalized over the fullerene cage, whereas in the latter the spin state of the endohedral cluster is altered, whereas the fullerene remains intact. Reproduced with permission from [18]

"non-innocent" ligand). In the second case, the endohedral cluster is the redox-active species, whereas the carbon cage merely acts as an inert container, transparent to electrons. In terms of organometallic electrochemistry, here the fullerene cage behaves as an innocent ligand, even though the electron transfer occurs across the metal/π-system interface. This type of electron transfer is described as an endohedral (or *in cavea*) electron transfer process [17, 18]. An obvious, but not always necessary, prerequisite for endohedral redox activity is a suitable energy of the metal-based molecular orbitals (MOs), which should be the frontier MOs (HOMO or LUMO) of the EMF molecule. Experimentally, the endohedral redox processes can be revealed via unexpected redox behavior (e.g., shifted potential when compared to analogous molecules) and/or with the use of spectroelectrochemical methods (such as electron spin resonance or nuclear magnetic resonance spectroelectrochemistry). In EPR spectra of ion-radicals, EMFs with endohedral redox activity often exhibit rich hyperfine structure with large coupling constants, as will be discussed in Chap. 9.

2.2 Monometallofullerenes

In monometallofullerenes (mono-EMFs), metal atoms transfer all valence electrons to the cage. The energies of metal-based electronic states are far from the frontier MOs, and hence HOMO and LUMO are completely localized on the fullerene cage, and redox activity of mono-EMFs is thus determined exclusively by the fullerene cage. As a result, redox properties are not strongly dependent on a particular metal, but are only determined by its valence state (i.e., the number of electrons transferred to the fullerene). Mono-EMFs usually exhibit electrochemically reversible reduction and oxidations.

$Li@C_{60}$ is the only $M^I@C_{60}$ EMF produced in sufficient amounts to be studied electrochemically. In a neutral state $Li@C_{60}$ is paramagnetic, and its stable form is the cation $Li^+@C_{60}$. Figure 2.1 shows that reduction behavior of $Li^+@C_{60}$ is similar to that of pristine C_{60} but with a cathodic shift of all reduction steps by ca 0.6 V [19]. Such a shift can be rationalized taking into account Coulomb interaction of electrons delocalized over the fullerene with the positive charge located in the center of the fullerene. Note that the data in Fig. 2.1 can be also described as that of $Li@C_{60}$. That is, the first reduction potential of $Li^+@C_{60}$ is the same as the first oxidation potential of $Li@C_{60}$. If considered this way, $Li@C_{60}$ appears to be easy to oxidize (−0.38 V) and easy to reduce (−0.95 V) due to an unpaired electron delocalized over the cage. The small gap_{EC} of $Li@C_{60}$, 0.47 V, is a common feature for paramagnetic mono-EMFs.

$M^{II}@C_{2n}$ mono-EMFs (M^{II} = Ca, Sm, Eu, Tm, Yb; $2n$ = 74–94) are diamagnetic molecules with closed-shell electronic structure. Their redox properties are comparable to those of higher empty fullerenes in that they are reasonably good

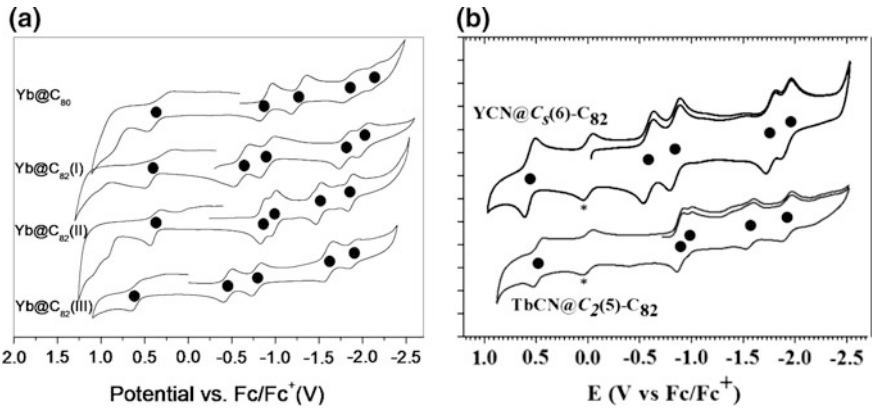

Fig. 2.3 **a** Cyclic voltammetry curves of $Yb@C_{80}$ and three isomers of $Yb@C_{82}$ (isomer I is $C_s(6)$, isomer II is $C_2(5)$, isomer III is $C_{2v}(9)$); reproduced with permission from [21]; **b** Cyclic voltammetry of $YbCN@C_{82}$-$C_s(6)$ and $TbCN@C_{82}$-$C_2(5)$; reproduced with permission from [29]. *Asterisk* denotes oxidation of ferrocene, *dots* denote EMF redox processes. Note similar redox potentials of $Yb@C_{82}$ and $(Tb,Y)CN@C_{82}$ EMFs with the same carbon cage isomers

electron acceptors (the first reduction potentials are more positive than −1 V), but at the same time their oxidation potentials are usually within the reach of standard conditions [20–28]. EC gaps of $M^{II}@C_{2n}$ EMFs typically exceed 1 V (Fig. 2.3b). Comparison of redox potentials of several Yb and Sm mono-EMFs with C_{82} cages (Table 2.1) shows that variation of redox potential due to the carbon cage isomerism can exceed 0.5 V. At the same time, variation of the metal has a minor influence (typically less than 0.05 V).

The redox behavior of $M^{III}@C_{2n}$ mono-EMFs (M^{III} is Sc, Y, La, Ce, Pr, Nd, Gd–Er, Lu) is substantially different from that of empty fullerenes and $M^{II}@C_{2n}$ EMFs because $M^{III}@C_{2n}$ molecules are radicals with an unpaired electron delocalized over the fullerene cage. As a result, their gap_{EC} values are usually close to

Table 2.1 Redox potentials of monometallofullerenes, their derivatives, and cyano-clusterfullerenes

EMF	Ox-II	Ox-I	Red-I	Red-II	Red-III	Gap_{ec}	References
C_{60}-I_h(1)		1.21	−1.12	−1.50	−1.95	2.33	[3]
C_{82}-C_2(3)		0.72	−0.69	−1.04	−1.58	1.41	[9]
$Li^+@C_{60}$-I_h(1)			−0.39	−0.98	−1.44		[19]
Yb@C_{82}-C_2(5)	0.90	0.38	−0.86	−0.98		1.24	[21]
Sm@C_{82}-C_2(5)		0.42	−0.84	−1.01	−1.51	1.26	[27]
Yb@C_{82}-C_s(6)		0.34	−0.62	−0.92	−1.81	0.96	[21]
Sm@C_{82}-C_{3v}(7)		0.56	−0.94	−1.25	−1.79	1.50	[26]
Yb@C_{82}-C_{2v}(9)		0.61	−0.46	−0.78		1.07	[21]
Sm@C_{82}-C_{2v}(9)		0.52	−0.42	−0.77	−1.60	0.94	[26]
TbCN@C_{82}-C_2(5)		0.50	−0.88	−0.97	−1.55	1.38	[29]
YCN@C_{82}-C_s(6)		0.56	−0.59	−0.84	−1.76	1.15	[30]
TbCN@C_{82}-C_s(6)		0.55	−0.59	−0.84	−1.77	1.14	[31]
TbCN@C_{82}-C_{2v}(9)		0.55	−0.46	−0.81	−1.78	1.01	[31]
La@C_{82}-C_s(6)	1.08	−0.07	−0.47	−1.40	−2.01	0.40	[5]
La@C_{82}-C_{2v}(9)	1.07	0.07	−0.42	−1.37	−1.53	0.49	[1]
Ce@C_{82}-C_{2v}(9)	1.08	0.08	−0.41	−1.41	−1.53	0.49	[3]
Gd@C_{82}-C_{2v}(9)	1.08	0.09	−0.39	−1.38	−2.22	0.48	[3]
Lu@C_{82}-C_{2v}(9)		0.11	−0.38	−1.17	−1.54	0.49	[32]
La@C_{82}-cycloadducts							
La@$C_{82}(Mes_2Si)_2CH_2$		−0.07	−0.50	−1.71	−1.75	0.43	[33]
La@C_{82}Ad	1.01	−0.07	−0.50	−1.71	−1.75	0.43	[34]
La@$C_{82}[C(COOEt)_2]$		0.08	−0.28	−1.19	–	0.36	[35]
La@C_{82}-R							
La@$C_{82}(C_6H_5CH_2)$-a		0.25	−0.68	−1.02	−1.21	0.93	[36]
La@$C_{82}(C_6H_5CH_2)$-d		0.15	−1.05	−1.15	−1.81	1.20	[36]
La@$C_{82}[CBr(COOEt)_2]$-A	0.85	0.38	−0.66	−1.31	−1.47	1.04	[35]

All values are measured in *o*-dichlorobenzene solution and are referred versus $Fe(Cp)_2^{+/0}$ pair

0.5 V, and such EMFs are normally easier to reduce or oxidize than empty fullerenes (Fig. 2.1, Table 2.1) [1, 3, 32, 37, 38]. The most studied are $M^{III}@C_{82}$ EMFs with $C_{2v}(9)$ cage isomer. Comparison of the redox potentials of such EMF with several different metals (Table 2.1) shows the values remain almost constant within the whole lanthanide row. Isomerism of the cage again has stronger influence: for instance, $C_s(6)$ isomer of $La@C_{82}$ is easier to oxidize than $C_{2v}(9)$ isomer by 0.14 V [5]. Interestingly, $M^{II}@C_{82}$-$C_{2v}(9)$ and $M^{III}@C_{82}$-$C_{2v}(9)$ have very similar reduction potentials, but oxidation potentials of $M^{III}@C_{82}$-$C_{2v}(9)$ are ca 0.4 V less positive.

Chemical derivatization of EMFs can significantly modify their redox potentials. Comparison of the redox properties of several derivatives of $La@C_{82}$-$C_{2v}(9)$ (Table 2.1) shows that derivatives can be divided into two groups. Cycloaddition (Diels–Alder, Bingel–Hirsch, bis-sylilation) does not change the paramagnetic state of the molecule, and hence the small gap_{EC} remains in the derivatives [33–35]. Redox potentials can be either positively or negatively shifted versus those of the parent $La@C_{82}$, depending on the addition site and the nature of the addend. On the other hand, when $La@C_{82}$ is functionalized by the groups forming single bond to the carbon cage (such as benzyl $C_6H_5CH_2$ or malonate $CBr(COOEt)_2$), the number of added groups is odd, and the carbon cage of the derivative becomes diamagnetic [35, 36]. Transformation of the open-shell structure of $La@C_{82}$ molecule to the closed-shell structure of the derivative strongly affects redox potentials. Oxidation potentials are shifted positively, whereas reduction potentials are shifted in the negative direction, and resulting gap_{EC} values usually exceed 1 V. Position of the group(s) on the cage may have strong influence on the exact values, as can be seen from comparison of the two isomer of $La@C_{82}(C_6H_5CH_2)$ with the difference of $E_{1/2}(0/-)$ values of 0.37 V [36].

2.3 Dimetallofullerenes

Whereas mono-EMFs show only cage-based redox properties, the encapsulation of two normally trivalent metal atoms (such as Sc, Y, La, and some lanthanides) within an EMF results in dimetallofullerenes (di-EMFs) with endohedral redox activity. The reason for the metal-based redox activity of $M_2@C_{2n}$ is the metal–metal bonding orbital (Figs. 2.4 and 2.5), which has a comparable energy to the frontier MOs of the carbon cage and can be either the HOMO or the LUMO of the di-EMF molecule.

Whether the M–M bonding MO in a given di-EMF involves the HOMO or the LUMO depends on the relative energies of the cage frontier MO and the energy of the metal–metal bonding orbital. It was shown that the energy of the M–M bonding MO in EMFs is similar to the lowest energy valence MO of the free metal dimer, which usually has $(ns)\sigma_g^2$ character [39]. The energy of the $(ns)\sigma_g^2$ orbital in the M_2 dimer correlates with the $ns^2(n-1)d^1 \rightarrow ns^1(n-1)d^2$ excitation energy of the free metal atom, and therefore this excitation energy to a large extent determines the

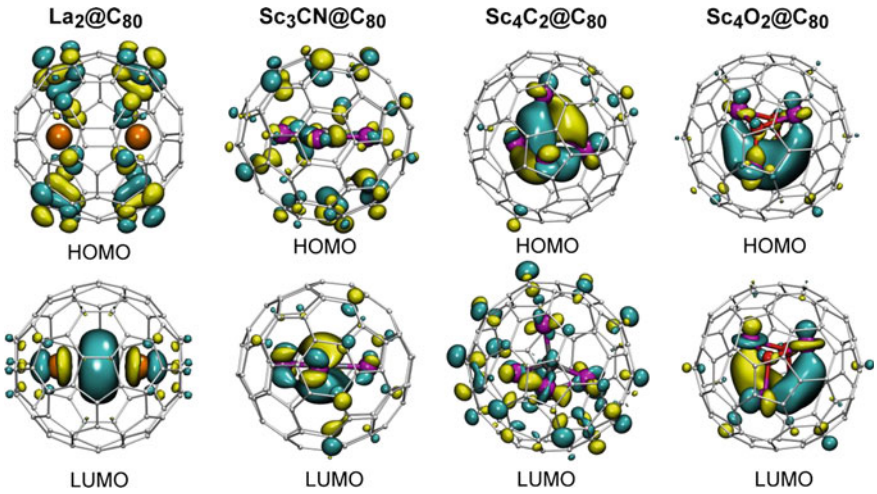

Fig. 2.4 DFT-computed frontier molecular orbitals (HOMO and LUMO) of several endohedral metallofullerenes with C_{80}-$I_h(7)$ carbon cage (formal charge of the cage −6): $La_2@C_{80}$, $Sc_3CN@C_{80}$, $Sc_4C_2@C_{80}$, and $Sc_4O_2@C_{80}$. Metals atoms are *orange* (La) or *magenta* (Sc)

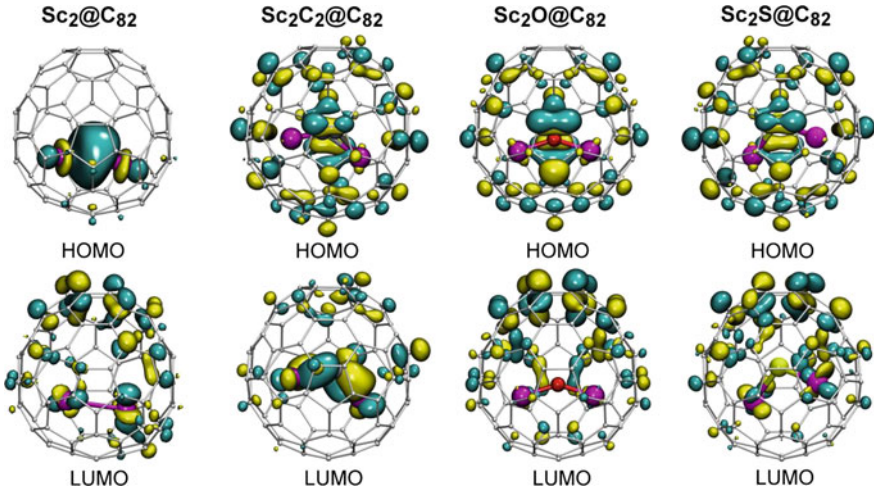

Fig. 2.5 DFT-computed frontier molecular orbitals (HOMO and LUMO) of several endohedral metallofullerenes with C_{82}-$C_{3v}(8)$ carbon cage (formal charge of the cage −4): $Sc_2@C_{82}$, $Sc_2C_2@C_{82}$, $Sc_2O@C_{82}$, and $Sc_2S@C_{82}$. Scandium atoms are *magenta*, oxygen is *red*, sulfur is *yellow*

valence state of metal atoms in di-EMFs. For instance, $ns^2(n-1)d^1 \rightarrow ns^1(n-1)d^2$ excitation energies increase in the row La–Sc/Y–Lu as 0.33–1.43/1.36–2.34 eV, respectively, and the $(ns)\sigma_g^2$ MO in corresponding M_2 dimers are stabilized in the row La_2–Sc_2/Y_2–Lu_2. As a result, in di-EMFs, La is always trivalent (the La–La

bonding MO is the LUMO in $(La^{3+})_2@C_{2n}^{6-}$), Lu tends to adopt a divalent state (the Lu–Lu bonding MO is the HOMO or even below the HOMO level in $(Lu^{2+})_2@C_{2n}^{4-}$), whereas the valence state of Sc, Y, and other lanthanides is more sensitive to the energy of the carbon cage MOs [39]. Figures 2.4 and 2.5 show frontier MOs of $La_2@C_{80}$-I_h(7) and $Sc_2@C_{82}$-C_{3v}(8) with M–M bonding LUMO and HOMO, respectively.

Since the La–La bonding MO is the LUMO in La-based di-EMFs (Fig. 2.4), reduction of a $La_2@C_{2n}$ molecules should be an endohedral redox process, whereas oxidation is expected to be fullerene-based. Electrochemical studies of $La_2@C_{2n}$ ($2n$ = 72, 78, 80) showed that these EMFs exhibit 2–3 reversible single-electron reduction steps and are relatively easy to reduce (Fig. 2.6). For instance, the first reduction of $La_2@C_{80}$-I_h occurs at −0.31 V [4]. Likewise, the first reductions of $La_2@C_{72}$ (−0.68) [40], $La_2@C_{78}$ (−0.40 V) [41], and $La_2@C_{80}$-D_{5h} (−0.36 V) [42] are also significantly more positive than for EMFs with fullerene-based reduction (Table 2.2). The first reduction potentials of analogous Ce di-EMFs are systematically more negative by up to 0.13 V (see Table 2.2) [42–45].

Metal-based reduction of $La_2@C_{80}$ is proved EPR spectroscopy. The M–M bonding orbitals in di-EMFs have hybrid *spd* character with large *s*-contribution. When such orbital is populated by a single electron, a hyperfine structure with large metal-based hyperfine constants can be expected in EPR spectra of corresponding anion-radicals. The EPR spectrum of the $[La_2@C_{80}$-$I_h]^-$ radical-anion exhibits a huge ^{139}La coupling constant of 364 G, which proves predominant localization of the spin density on the metals (see Chap. 8 for more details on EPR spectroscopy of $La_2@C_{80}$ anion and derivatives) [48]. Another indication of the endohedral reduction in La and Ce di-EMFs is the difference between the first and the second reduction potentials. For a cage-based redox process, the difference between the first and second reduction (or oxidation) steps is usually within 0.4–0.5 V range if the process is based on the same cage MO (see Table 2.1 for reduction potentials of C_{60}, C_{82} etc.). An endohedral redox process results in a much larger potential difference for the consequent redox steps, since these steps are either based on the

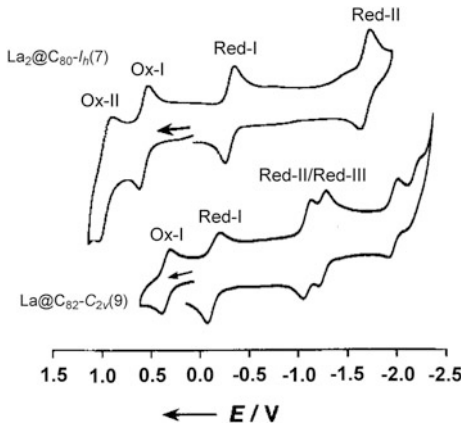

Fig. 2.6 Cyclic voltammetry of $La_2@C_{80}$-I_h(7) compared to that of $La@C_{82}$-C_{2v}(9); scan rate 20 mV/s, *o*-dichlorobenzene solution. Reproduced with permission from [4] and [1]

Table 2.2 Redox potentials of representative di-EMFs

EMF	Ox-II	Ox-I	Red-I	Red-II	Red-III	Gap_{EC}	References
$La_2@C_{72}$-D_2(10611)	0.75	0.24	−0.68	−1.92	–	0.92	[40]
$Ce_2@C_{72}$-D_2(10611)	0.82	0.18	−0.81	−1.86		0.99	[43]
$La_2@C_{76}$-C_s(17490)	0.65	0.21	−0.63	−1.83	−2.40	0.84	[46]
$La_2@C_{78}$-D_{3h}(5)	0.62	0.26	−0.40	−1.84	−2.28	0.66	[41]
$Ce_2@C_{78}$-D_{3h}(5)	0.79	0.25	−0.52	−1.86	−2.23	0.77	[44]
$La_2@C_{80}$-D_{5h}(6)	0.78	0.22	−0.36	−1.72		0.58	[42]
$Ce_2@C_{80}$-D_{5h}(6)	0.66	0.20	−0.40	−1.76	−2.16	0.60	[42]
$La_2@C_{80}$-I_h(7)	0.95	0.56	−0.31	−1.72		0.87	[4]
$Ce_2@C_{80}$-I_h(7)	0.95	0.57	−0.39	−1.71	–	0.96	[45]
			–	–	–		
$Gd_2@C_{79}N$-I_h(7)		0.51	−0.96	−1.98	–	1.45	[47]

cluster MO (which has a much higher on-site Coulomb interaction than in the fullerene cage) or affect different MOs (one on the cluster and one on the carbon cage). The difference between the first and the second reduction potentials in all $La_2@C_{2n}$ and $Ce_2@C_{2n}$ di-EMFs is in the range of 1.23–1.44 V (Table 2.2), which is much larger than for consequent cage-based reductions.

Substituting one carbon atom for a nitrogen atom in $M_2@C_{80}$-I_h results in paramagnetic azafullerenes $M_2@C_{79}N$ (M = Y, Tb, Gd) [47, 49]. The SOMO of these molecules is an M–M bonding MO similar to the anion radicals of $La_2@C_{80}$. In line with this MO analysis, the ESR study of $Y_2@C_{79}N$ revealed an enhanced ^{89}Y hfc constant of 81.2 G (see Chap. 7 for more details on EPR spectra of $Y_2@C_{79}N$) [49]. An electrochemical study of $Gd_2@C_{79}N$ showed that its first reduction potential, −0.96 V, is not as positive as that of $La_2@C_{80}$-I_h. However, the second reduction of $Gd_2@C_{79}N$ is found at −1.98 V, i.e., the difference between the first and second reduction potentials is as large as 1.02 V. Based on redox potentials and DFT calculations, which predict a Gd_2-localized LUMO, the first reduction of $Gd_2@C_{79}N$ can be tentatively assigned to an endohedral reduction. Interestingly, the M–M bonding SOMO in $M_2@C_{79}N$ is "buried" below the cage-based MOs, and hence oxidation of $M_2@C_{79}N$ should be a cage-based process [47, 49]. Indeed, the oxidation potential of $Gd_2@C_{79}N$ is +0.51 V, which is close to the value of $La_2@C_{80}$-I_h (+0.56) with cage-based oxidation.

Metal-based oxidation and fullerene-based reduction can be expected for di-EMFs with metal-based HOMO, such as $M_2@C_{82}$ di-EMFs (M = Sc, Lu, Y etc.). The information on electrochemical behavior of such di-EMFs is rather limited, and the proof of the metal-based oxidation is not as straightforward as for La-based di-EMFs. The most illustrative in such situation is comparison with redox behavior of other EMFs, with the same carbon cage in the same formal charge state. Figure 2.5 compares frontier MOs of $Sc_2@C_{82}$, $Sc_2C_2@C_{82}$, $Sc_2O@C_{82}$, and $Sc_2S@C_{82}$, all with the C_{82}-C_{3v}(8) cage isomer in the formal charge of −4. It can be seen that in the whole series, the HOMO of $Sc_2@C_{82}$ is localized on the endohedral

scandium dimer, whereas the HOMO of other clusterfullerenes is mainly fullerene based. At the same time, the LUMO of $Sc_2@C_{82}$ as well as that of $Sc_2O@C_{82}$ and $Sc_2S@C_{82}$ is localized on the fullerene cage. Based on the MO analysis, similar reduction potentials can be expected for $Sc_2@C_{82}$ and clusterfullerenes due to the same nature of electron-accepting orbital, whereas oxidation potential of $Sc_2@C_{82}$ should be more negative than in other clusterfullerenes because of the higher energy of the Sc–Sc bonding MO than that of the cage MO. Indeed, oxidation potential of $Sc_2@C_{82}$-C_{3v}(8), +0.05 V [50], is considerably less positive than that of $Sc_2C_2@C_{82}$ (+0.47 V) [51], $Sc_2O@C_{82}$ (+0.54 V) [52], or $Sc_2S@C_{82}$ (+0.52 V) [53], whereas their reduction potentials are more similar (Table 2.3). Definitive proof of the Sc-based oxidation of $Sc_2@C_{82}$ is provided by EPR spectrum of its radical-cation with a huge ^{45}(Sc) hfc constant of 199 G (see Chap. 9).

Since the energy of the $(ns)\sigma_g^2$ orbital in the M_2 dimer and hence the energy of the M–M bonding orbital in di-EMFs correlates with the $ns^2(n-1)d^1 \rightarrow ns^1(n-1)d^2$ excitation energy of the free metal atom, the oxidation potentials of di-EMFs with M–M bonding HOMO can be expected to vary with the metal. In

Table 2.3 Redox potentials of representative EMFs with 4-fold charged cluster (oxide, sulfide, and carbide clusterfullerenes and dimetallofullerenes)

EMF	Ox-II	Ox-I	Red-I	Red-II	Red-III	Gap_{ec}	References
$Sc_2O@C_{70}$-C_2(7892)	0.55	0.10	−1.36	−1.80	−	1.46	[54]
$Sc_2S@C_{70}$-C_2(7892)	0.65	0.14	−1.44	−1.87	−1.99	1.58	[55]
$Sc_2C_2@C_{72}$-C_S(10528)		0.41	−1.19	−1.54	−1.75	1.60	[56]
$Sc_2S@C_{72}$-C_S(10528)	1.21	0.64	−1.14	−1.53	−2.24	1.78	[57]
$Sc_2O@C_{76}$-T_d(1)		0.32	−0.91	−1.40	−1.65	1.23	[58]
$Sc_2C_2@C_{80}$-C_{2v}(5)		0.41	−0.74	−1.33	−	1.15	[59]
$Sc_2O@C_{80}$-C_{2v}(5)	0.56	0.24	−0.89	−1.48	−1.75	1.13	[60]
$Er_2@C_{82}$-C_s(6)	0.65	0.02	−1.01	−1.31	−	1.03	[61]
$Lu_2@C_{82}$-C_s(6)	0.74	0.34	−1.00	−1.32	−1.77	1.34	[61]
$Sc_2C_2@C_{82}$-C_s(6)	0.64	0.42	−0.93	−1.30	−	1.35	[62]
$Sc_2O@C_{82}$-C_s(6)	0.72	0.35	−0.96	−1.28	−1.74	1.31	[53]
$Sc_2S@C_{82}$-C_s(6)	0.65	0.39	−0.98	−1.12	−1.73	1.37	[53]
$Er_2S@C_{82}$-C_s(6)		0.39	−1.01	−1.85	−2.21	1.40	[61]
$Sc_2@C_{82}$-C_{3v}(8)		0.05	−1.10	−		1.15	[50]
$Er_2@C_{82}$-C_{3v}(8)		0.13	−1.14	−1.41	−1.83	1.27	[61]
$Lu_2@C_{82}$-C_{3v}(8)	0.95	0.50	−1.16	−1.46	−1.77	1.66	[61]
$Sc_2C_2@C_{82}$-C_{3v}(8)	0.93	0.47	−0.94	−1.15	−1.60	1.41	[51]
$Sc_2O@C_{82}$-C_{3v}(8)	1.09	0.54	−1.17	−1.44	−1.55	1.71	[52]
$Sc_2S@C_{82}$-C_{3v}(8)	0.96	0.52	−1.04	−1.19	−1.63	1.56	[53]
$Er_2S@C_{82}$-C_{3v}(8)	0.88	0.51	−0.98	−1.21	−1.70	1.49	[61]
$Sc_2C_2@C_{82}$-C_{2v}(9)	0.67	0.25	−0.74	−0.96		0.99	[63]
$Sc_2C_2@C_{86}$-C_{2v}(9)		0.47	−0.84	−1.11	−1.63	1.31	[64]

All values are measured in *o*-dichlorobenzene solution and are referred versus $Fe(Cp)_2^{+/0}$ pair

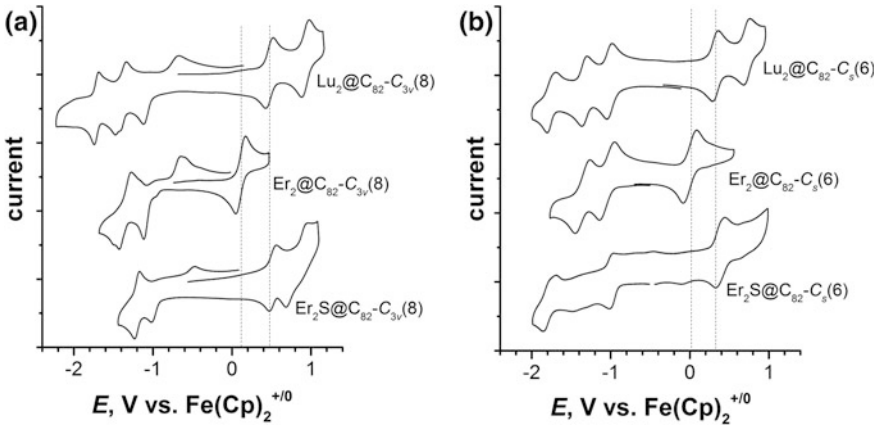

Fig. 2.7 **a** Cyclic voltammetry of a series of $Lu_2@C_{82}$, $Er_2@C_{82}$, and $Er_2S@C_{82}$, all with C_{82}-$C_{3v}(8)$ cage isomer; **b** isomeric EMFs with C_{82}-$C_s(6)$ cage. Scan rate 100 mV/s, *o*-dichlorobenzene solution

particular, Lu with the lowest energy of this MO should have the highest oxidation potential. Indeed, whereas reduction potentials of $Er_2@C_{82}$ and $Lu_2@C_{82}$ are close to each other and to that of $Er_2S@C_{82}$, their oxidation potentials are substantially different: $Er_2@C_{82}$ is easier to oxidize than $Lu_2@C_{82}$ by 0.36 V (see Fig. 2.7 and Table 2.3 for comparison of cyclic voltammetry curves and redox potentials). Furthermore, the first oxidation potential of $Lu_2@C_{82}$ is close to that of $Er_2S@C_{82}$, which has fullerene-based oxidation. Similar redox properties are observed for C_{82}-$C_s(6)$ cage isomers of these EMFs (Table 2.3). Thus, due to the metal-based redox process, oxidation potentials of di-EMFs are subject to significant variation in dependence on the encapsulated metal.

2.4 Clusterfullerenes

Electrochemical properties of clusterfullerenes (CFs), i.e., endohedral metallofullerenes whose endohedral species comprise metal and nonmetal atoms, may vary significantly in dependence on the formal charges and spatial localization of frontier MOs. Typical formal charges of endohedral cluster are +2 (cyano-clusterfullerenes with single metal, such as $YCN@C_{82}$ and $TbCN@C_{82}$), +4 (carbide CFs $M_2C_2@C_{2n}$, sulfide CFs $M_2S@C_{2n}$, oxide CFs $M_2O@C_{2n}$), or +6 (nitride CFs $M_3N@C_{2n}$, methano-CF $Sc_3CH@C_{80}$, μ^3-carbido CF $M_2TiC@C_{80}$, oxide CF $Sc_4O_2@C_{80}$, and many other EMFs, see Chap. 1 for a complete list).

Clusterfullerenes with formal charge +2. Redox potentials of $MCN@C_{82}$ are similar to those of corresponding cage isomers of mono-EMFs with divalent metals, $M^{II}@C_{82}$ with corresponding cage isomers (Refs. [29–31], see Table 2.1). This

close similarity indicates that the fullerene cage has the dominant contribution to HOMO and LUMO of these clusterfullerenes. Reduction and oxidation steps are usually reversible, similar to those of mono-EMFs (Fig. 2.3).

Oxide, carbide, and sulfide clusterfullerenes with fourfold charged clusters. For clusterfullerenes with +4 charge, the most typical cages are C_{82}-$C_{3v}(8)$ and C_{82}-$C_s(6)$. Figure 2.5 compares frontier MOs of the carbide CF $Sc_2C_2@C_{82}$, oxide CF $Sc_2O@C_{82}$, and sulfide CF $Sc_2S@C_{82}$, all with the C_{82}-$C_{3v}(8)$ cage isomers. In these molecules, the HOMOs are predominantly localized on the carbon cage, which results in close values of their oxidation potentials at 0.47–0.54 V (Table 2.3), significantly more positive that the first oxidation potential of the di-EMF $Sc_2@C_{82}$ with the same carbon cage isomer but metal-based HOMO. The LUMO distributions of these CFs show a subtle balance between the fullerene and the cluster: the LUMO of $Sc_2O@C_{82}$ is localized on the fullerene, the LUMO of $Sc_2S@C_{82}$ is also largely fullerene-based but with noticeable metal contributions, whereas the LUMO of $Sc_2C_2@C_{82}$ is predominantly localized on the carbide cluster. The first reduction potentials follow the order of the cage contribution to the LUMOs: the most negative value is reported for $Sc_2O@C_{82}$ (−1.17 V) [52] followed by $Sc_2S@C_{82}$ (−1.04 V) [53] and then by $Sc_2C_2@C_{82}$ (−0.94 V) [51]. Similar correlations between redox potential and endohedral cluster can be revealed for analogous CFs with C_{82}-$C_s(6)$ cages (Table 2.3). Remarkably, CFs with C_{82}-$C_{3v}(8)$ and $C_s(6)$ cages exhibit different electrochemical behavior in terms of reversibility: whereas EMFs with $C_s(6)$ cage have reversible reductions, those of EMFs with $C_{3v}(8)$ cage are electrochemically irreversible (Fig. 2.7). In fact, low electrochemical reversibility of reduction and oxidation steps is rather common for CFs, and we will return to this point below, in the discussion of nitride CFs.

Information on electrochemical properties of carbide, sulfide, or oxide CFs with other cage sizes is rather limited. All data available at the moment of mid 2016 are compiled in Table 2.3. Typically, compounds exhibit reasonably high gap_{EC} (exceeding 1 V) and irreversible reduction behavior. When different clusters are available within the same fullerene cage, redox potential are usually rather similar.

Nitride Clusterfullerenes. Figure 2.8 shows frontier MOs of nitride clusterfullerenes $Sc_3N@C_{80}$-I_h and $Y_3N@C_{80}$-I_h. $Y_3N@C_{80}$ with fullerene-based HOMO and LUMO represents a typical situation for a majority of nitride CFs. On the contrary, high electronegativity of Sc results in rather unique situation for $Sc_3N@C_{80}$, whose LUMO has large cluster contribution. Furthermore, there is a structural flexibility caused by rotation of the M_3N cluster inside the cage, which also affects spatial localization of the LUMO. Computational studies showed that in the neutral state, $Sc_3N@C_{80}$ and $Y_3N@C_{80}$ both have C_3-symmetric configuration, in which metal atoms are facing hexagons in quasi-η^6 manner (albeit somewhat shifted from the center of hexagons to pentagon/hexagon edges) [65]. In the anionic state, C_{3v}-symmetric configuration with metals η^2-coordinating centers of pentagon/hexagon edges is preferred for $Sc_3N@C_{80}$. Importantly, rotation of the cluster in $Sc_3N@C_{80}$ results in dramatic redistributing of the LUMO: in the C_3-conformer, the orbitals is equally shared between the cage and the cluster, whereas in the C_{3v}-conormer the cluster has dominant contribution to the LUMO

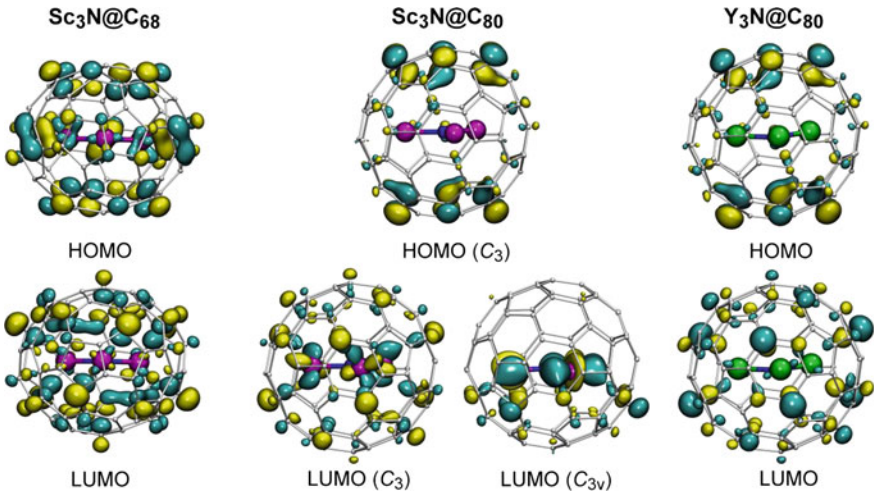

Fig. 2.8 Frontier molecular orbitals (HOMO and LUMO) of $Sc_3N@C_{68}$-D_3(6140), $Sc_3N@C_{80}$-I_h(7), and $Y_3N@C_{80}$-I_h(7). The LUMO of $Sc_3N@C_{80}$ is show for two conformers: C_3-conformer is the lowest energy for the neutral state, whereas C_{3v}-conformer is the lowest energy for the anion. For $Y_3N@C_{80}$, C_3-conformer has the lowest energy in both neutral and anionic states

(Fig. 2.8). For $Y_3N@C_{80}$, C_{3v}-conformer is much higher in energy due to the larger size of the cluster, and the C_3-conformer with dominant cage contribution to the LUMO remains the ground state for both neutral and anionic forms.

Based on the spatial distribution of frontier orbitals, one can expect similar anodic and different cathodic behavior of $Sc_3N@C_{80}$ and $Y_3N@C_{80}$. Indeed, both EMFs have similar oxidation potential near 0.6 V, but noticeably different reduction potentials, −1.26 V for $Sc_3N@C_{80}$ and −1.41 for $Y_3N@C_{80}$. $Sc_3N@C_{80}$ is reduced mainly at its endohedral cluster, as was also proved by the EPR spectrum of its anion radical [66]. $Y_3N@C_{80}$ is reduced predominantly at its fullerene cage, and its reduction potential can be considered as a reference point for cage-based reduction in EMFs with C_{80}-I_h cage. Not only reduction potential of the two nitride CFs is different, they also have a different reversibility of the process. At modest voltammetric scan rates both EMFs exhibit electrochemically irreversible but chemically reversible reduction. That is, reduction is followed by a chemical reaction, which can be reversed at positive potentials so that pristine EMF is restored. However, in $Sc_3N@C_{80}$ electrochemical reversibility of the first reduction can be achieved at scan rates of several V/s (Fig. 2.9), whereas in $Y_3N@C_{80}$ and many other nitride CFs the first reduction remains electrochemically irreversible up to the scan rates of at least 70 V/s [67, 68].

The nature of the follow-up reaction in reduction of nitride CFs was debated for quite a long time. Reaction with solvent or decomposition of nitride CFs upon reduction can be excluded by chemical reversibility of the reduction. Hypothesis of dimerization of anion-radicals was proposed in 2008 based on ESR

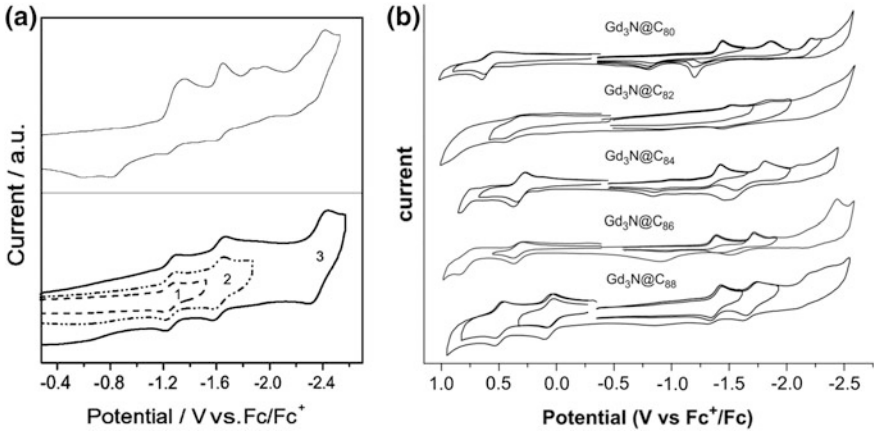

Fig. 2.9 **a** Cyclic voltammograms of $Sc_3N@C_{80}$-I_h(7) in *o*-dichlorobenzene at scan rates of 100 mV/s in the upper panel, and 6 V/s (1), 10 V/s (2), and 20 V/s (3) in the lower panel. The different scan rates for each reduction reflect the scan rate necessary to achieve full electrochemical reversibility. Reproduced with permission from [69]; **b** cyclic voltammograms of the $Gd_3N@C_{2n}$ family measured in *o*-dichlorobenzene at 100 mV/s. Reproduced from Ref. [70]

spectroelectrochemical studies of $Sc_3N@C_{68}$ [71]. Although radical-anion and radical-cation could be detected by ESR upon reduction and oxidation, respectively, integral intensity of the radical-anion was an order of magnitude lower in the same experimental conditions. This fact indicated that the main product of the reduction was diamagnetic, and reversible formation of the single-bonded $(Sc_3N@C_{68}^{-})_2$ dimer was proposed. DFT computations showed that dimerization of anion radicals of nitride CFs is more energetically favorable than that of empty fullerenes [72]. Recently, a strong argument in favor of dimerization hypothesis was provided by an observation of $(Sc_3N@C_{80}^{-})_2$ dimers in the single-crystal X-ray diffraction study of the anion-radical $Sc_3N@C_{80}^{-}$ crystallized with cryptand [2,2,2] (Na^+) cation [73].

Electrochemical properties of nitride CFs were studied in a lot of details, with many cage sizes and different metals in nitride clusters (Table 2.4). For Sc-based nitride CFs, available cages are C_{68}, C_{78}, two isomers of C_{80}, and C_{82}. Remarkably, $Sc_3N@C_{80}$-I_h has the highest oxidation potential among the series, whereas the first oxidation potential of another isomer, $Sc_3N@C_{80}$-D_{5h}, is 0.25 V more negative. The difference in oxidation potentials of the two isomers was used by Echegoyen et al. for their facile separation [69]. Redox behavior of $Sc_3N@C_{68}$ was studied especially carefully, and cage-based reduction and oxidation were confirmed by EPR spectroelectrochemistry in agreement with DFT-predicted localization of HOMO and LUMO on the carbon cage (Fig. 2.8) [71].

For medium size nitride clusters, such as exemplified by Gd_3N in Table 2.4 and Fig. 2.9, cages from C_{78} to C_{88} were studied electrochemically (note that C_{78} and C_{82} cage isomers for Sc_3N and Gd_3N are different). Even larger cages, up to C_{96}, were studied for large lanthanides such as La or Ce. Redox properties of all these

Table 2.4 Redox potentials of representative nitride clusterfullerenes

EMF	Ox-II	Ox-I	Red-I	Red-II	Red-III	Gap_{ec}	References
$Sc_3N@C_{68}$-D_3(6140)	0.85	0.33	−1.45	−2.05		1.78	[74]
$Sc_3N@C_{78}$-D_{3h}(5)	0.68	0.21	−1.56	−1.91		1.77	[75]
$Sc_3N@C_{80}$-D_{5h}(6)		0.34	−1.33			1.68	[76]
$Sc_3N@C_{80}$-I_h(7)	1.09	0.59	−1.26	−1.62	−2.37	1.85	[69]
$Sc_3N@C_{82}$-C_{2v}(9)	0.37	0.00	−1.35	−1.52	−1.78	1.35	[77]
$Gd_3N@C_{78}$-C_2(22010)	1.00	0.47	−1.53	−1.89		2.00	[78]
$Gd_3N@C_{80}$-I_h(7)		0.58	−1.44	−1.86	−2.13	2.02	[79]
$Gd_3N@C_{82}$-C_s(39663)		0.38	−1.53	−1.87		1.91	[70]
$Gd_3N@C_{84}$-C_s(51365)		0.32	−1.37	−1.76		1.69	[79]
$Gd_3N@C_{86}$-D_3(17)		0.33	−1.39	−1.72		1.82	[70]
$Gd_3N@C_{88}$-D_2(35)	0.45	0.05	−1.39	−1.71		1.49	[80]
$Ce_3N@C_{88}$-D_2(35)	0.63	0.08	−1.30	−1.57		1.38	[81]
$Ce_3N@C_{92}$-T(92)		0.32	−1.48	−1.64		1.80	[82]
$Ce_3N@C_{96}$-D_2(186)	0.67	0.18	−1.50	−1.84		1.68	[83]

All values are measured in *o*-dichlorobenzene solution and are referred versus $Fe(Cp)_2^{+/0}$ pair

NCFs are to some extent similar to the properties of $M_3N@C_{80}$-I_h(7). The first (and sometimes also the second) oxidation step is usually reversible, while reduction steps are electrochemically irreversible. Variation of redox potentials of different NCFs with the same carbon cage hardly exceeds 0.1 V and is usually smaller (except for Sc). With variation of the carbon cages, reduction potentials also do not show significant changes, whereas oxidation potentials seem to shift cathodically with the increase of the cage size, so that the electrochemical gap tends to be smaller for larger cages, from 2.0 V for $M_3N@C_{78}$-C_2(22010) to ca 1.7 V for $M_3N@C_{96}$. Redox properties of $M_3N@C_{88}$-D_2(35) NCFs fall apart from the others in that it is the only group of NCFs which exhibits electrochemically reversible reductions and the most cathodically shifted oxidation near +0.05 V.

Derivatives of $Sc_3N@C_{80}$. Chemical derivatization (such as cycloaddition or radical addition) and its influence on electrochemical properties of nitride CFs has been studied very extensively, especially for $Sc_3N@C_{80}$-I_h. Table 2.5 compares redox potentials of several derivatives of the latter. There are at least two factors which determine how redox potentials are changed in the derivative when compared to the pristine EMFs. First, topology of the π-system of the fullerene is changed in its derivatives, which substantially influence the energies of frontier MOs. Second, the energies of the frontier MOs can be influenced by an electron-donating or electron-withdrawing nature of the addends.

Highly symmetrical C_{80}-I_h fullerene has only two types of bonds at which cycloaddition can occur: pentagon/hexagon edge (denoted as [5,6]) and hexagon/hexagon edge (denoted as [6,6]). Besides, the sigma-bond at the functionalized edge can remain intact (then the cycloadduct is "closed") or it can be broken (then the cycloadduct is "open"). Thus, four types of cycloadducts can be

Table 2.5 Redox potentials of $Sc_3N@C_{80}$-I_h derivatives

$Sc_3N@C_{80}$ derivative	Ox-II	Ox-I	Red-I	Red-II	Red-III	Gap_{EC}	References
$Sc_3N@C_{80}$-I_h(7)	1.09	0.59	−1.26	−1.62	−2.37	1.85	[69]
[5,6]-closed $Sc_3N@C_{80}$-pyrrolidine (N-ethyl)		0.62	−1.18	−1.57	−2.29	1.80	[84]
[5,6]-closed $Sc_3N@C_{80}$-Diels–Alder		0.62	−1.16	−1.54	−2.26	1.78	[84]
[5,6]-closed $Sc_3N@C_{80}(C_6H_4)$	0.92	0.34	−1.11	−1.50	−2.21	1.45	[85]
[6,6]-closed $Sc_3N@C_{80}(C_6H_4)$	0.83	0.42	−1.08	−1.29	−2.23	1.50	[85]
[6,6]-open $Sc_3N@C_{80}$-methano-$C(CO_2Et)_2$	1.08	0.56	−1.34	−1.90	−2.22	1.90	[86]
[6,6]-open $Sc_3N@C_{80}$-methano-(CHPh)	1.08	0.50	−1.48	−2.01	−2.40	1.98	[87]
[6,6]-open $Sc_3N@C_{80}$-PCBM	1.15	0.52	−1.33	−1.91	–	1.85	[88]
1,4-$Sc_3N@C_{80}(Mes_2Si)_2CH_2$		0.08	−1.45	–	–	1.53	[89]
1,4-$Sc_3N@C_{80}(CF_3)$	1.66	0.43	−1.16	−1.65	−2.14	1.59	[90]
$Sc_3N@C_{80}(CF_3)_4$		0.55	−1.06	−1.55	−2.03	1.61	[91]
$Sc_3N@C_{80}(CF_3)_{10}$		0.86	−0.84	−1.32	−2.11	1.70	[91]
$Sc_3N@C_{80}(CF_3)_{12}$		0.95	−0.95	−1.38	−1.98	1.90	[91]

All values are measured in *o*-dichlorobenzene solution and are referred versus $Fe(Cp)_2^{+/0}$ pair

expected for $Sc_3N@C_{80}$-I_h: [5,6]-open, [5,6]-closed, [6,6]-open, and [6,6]-closed. Electrochemical data is available for three of them, whereas [5,6]-open cycloadducts (which are very rare) have not been studied by electrochemistry so far. [5,6]-closed adducts are the most abundant products of cycloaddition to $Sc_3N@C_{80}$ in Prato or Diels–Alder reactions. Remarkably, they exhibit reversible reductions (as opposed to electrochemically irreversible reductions of pristine $Sc_3N@C_{80}$) [84, 85]. In all three [5,6]-closed adducts listed in Table 2.5, the first reduction is more positive than that of $Sc_3N@C_{80}$. Oxidation potential is virtually not affected by the addend. [6,6]-closed adducts also exhibit reversible reduction behavior, and their reduction potentials are slightly more positive than in analogous [5,6]-closed adducts, as can be concluded from the comparison of two isomers of $Sc_3N@C_{80}(C_6H_4)$ benzoadducts [85]. [6,6]-open adducts (such as those obtained in Bingel–Hirsch reaction or PCBM-like-derivatives of $Sc_3N@C_{80}$) exhibit distinctly different electrochemical behavior: their reductions are irreversible and occur at more negative potentials than in $Sc_3N@C_{80}$.

Reaction of $Sc_3N@C_{80}$ with two bulky radical groups (such CF_3 or benzyl) or its bis-silylation result in 1,4-addition to one of the fullerene hexagons. Comparison of two derivatives with 1,4-addition pattern, $Sc_3N@C_{80}(CF_3)_2$ and $Sc_3N@C_{80}(Mes_2Si)_2CH_2$ (Mes = mesityl), shows how the electronic properties of the addends can affect redox potentials [89, 90]. Strongly electron-donating $(Mes_2Si)_2CH_2$ shifts reduction and oxidation potentials negatively with respect to the $Sc_3N@C_{80}$ values, whereas electron-withdrawing CF_3 groups move redox

potentials positively [89, 90]. As a result, the difference of the first reduction potentials of the two derivatives (which is solely due to the electron-donating/withdrawing effects) is as large as 0.29 V. Note that both derivatives exhibit reversible reduction steps. Interestingly, multiple CF_3 addition shifts the first reduction potential further in the positive direction up to $Sc_3N@C_{80}(CF_3)_{10}$ ($E_{1/2}(0/-) = -0.84$ V), whereas for $Sc_3N@C_{80}(CF_3)_{12}$ the effect is reversed ($E_{1/2}(0/-) = -0.95$ V), presumably because saturation of the π-system outweighs the electron-withdrawing effect of CF_3 groups [91].

Mixed-metal nitride clusterfullerenes with electroactive metals. Nitride clusterfullerenes provide a convenient platform for creating redox-active endohedral cluster via formation of the mixed-metal clusters with redox-active metals. Three such metals were incorporated in nitride CFs so far: cerium, titan, and vanadium.

Ce is different from all other lanthanides in that its Ce^{IV} valence state is accessible and known for a plethora of inorganic and organometallic compounds, and redox potential of the Ce^{IV}/Ce^{III} couple can vary in a broad range [92]. However, redox behavior of Ce-based mono- and di-EMFs as well as Ce_3N-nitride CFs was found to be very similar to that of La-counterparts, suggesting that Ce^{III} in EMFs is electrochemically inert. The first indication that endohedral Ce can be redox active was obtained in 2010 with isolation of $CeLu_2N@C_{80}$-I_h [93]. Its first oxidation potential at 0.01 V was ca 0.6 V more negative than expected for a fullerene-based oxidation in $M_3N@C_{80}$-I_h nitride CF, which was interpreted as an oxidation of endohedral Ce^{III}. DFT computational study also showed that removal of the $4f^1$ electron from Ce is more energetically favorable (i.e., gives lower ionization potential) than removal of an electron from the fullerene cage.

In a follow-up study, Sc and Y were chosen to vary the size of the endohedral cluster in the $CeM_2N@C_{80}$ series (Shannon's radii of Sc^{3+}, Lu^{3+}, and Y^{3+} ions are 0.745, 0.86, and 0.90 Å, respectively) [94]. Figure 2.10a shows cyclic voltammograms of three $CeM_2N@C_{80}$-I_h NCFs compared to $PrSc_2N@C_{80}$-I_h (the latter was chosen as a reference because of the close ionic radii of Ce^{3+}, 1.01 Å, and Pr^{3+}, 0.99 Å). Whereas cathodic behavior with the first reduction near −1.36 V is similar for all four EMFs, their anodic behavior is quite different (Table 2.6). $CeM_2N@C_{80}$ compounds exhibit one reversible oxidation step whose potential varies from –0.07 V for $CeY_2M@C_{80}$ to +0.33 V for $CeSc_2N@C_{80}$. The latter is still 0.31 V more negative than the oxidation potential of $PrSc_2N@C_{80}$, hence indicating a Ce-based redox process. Compelling evidence of the endohedral oxidation of Ce^{III} in $CeM_2N@C_{80}$-I_h NCFs was provided by NMR spectroscopy of the $CeM_2N@C_{80}^+$ cations obtained by chemical oxidation (Fig. 2.10b). The NMR study showed that cations are diamagnetic, which is possible only in case of endohedral $Ce^{III} \rightarrow Ce^{IV}$ oxidation (cage-based oxidation would produce radicals with non-detectable NMR signals). The metal dependence of the oxidation potential can be explained by a buildup of an inner strain in the $CeM_2N@C_{80}$ row with increasing the cluster size from $CeSc_2N$ to CeY_2N. The strained is caused by the limited interior space inside the C_{80}-I_h cage, and the increase of the ionic radius of M^{3+} in the Sc → Lu → Y series makes the corresponding $CeM_2N@C_{80}$ more

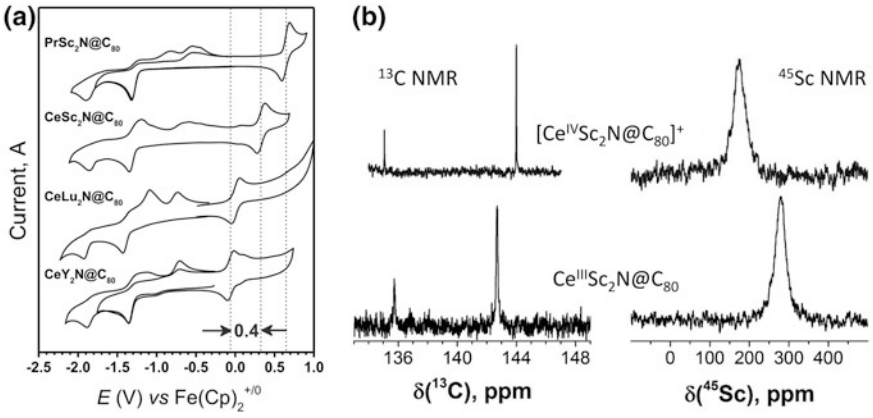

Fig. 2.10 **a** Cyclic voltammetry $PrSc_2N@C_{80}$-I_h(7) and $CeM_2N@C_{80}$-I_h(7) (M = Sc, Lu, and Y) (scan rate 100 mV/s, *o*-dichlorobenzene solution). Strong negative shift of the oxidation potential on coming from $PrSc_2N@C_{80}$ (fullerene-based oxidation) to $CeSc_2N@C_{80}$ (Ce-based oxidation) is observed. Further negative shift in the $CeM_2N@C_{80}$ series is caused by the increased *inner strain* with the increase of the metal size. **b** ^{13}C and ^{45}Sc NMR spectra of pristine and oxidized $CeSc_2N@C_{80}$ in *o*-dichlorobenzene solution. Based on the data from [94]

prone to oxidation as a way to release the strain (ionic radius of Ce^{4+}, 0.87 Å, is considerably smaller than that of Ce^{3+}). Therefore, the oxidation potential of $CeM_2N@C_{80}$-I_h shifts to more negative values for larger M^{3+} ions.

The concept of the strain-driven Ce^{IV}/Ce^{III} endohedral redox couple was further developed in the study of $Ce_xM_{3-x}N@C_{2n}$ nitride CFs with different cages and cluster compositions (x = 1, 2; M = Sc or Y; $2n$ = 78, 84, 86, 88) [95]. Redox potentials were determined for 12 Ce-containing NCFs and compared to the non-Ce analogs. On the basis of the shift of the oxidation potential and an increased difference between the first and second oxidation potentials, an endohedral $Ce^{III} \rightarrow Ce^{IV}$ redox process at the first oxidation step was proven for $CeSc_2N@C_{78}$, $CeY_2N@C_{84}$, and $Ce_2YN@C_{86}$. Less confidently, an endohedral oxidation of Ce was also proposed for $Ce_2ScN@C_{86}$, $CeY_2N@C_{86}$, and $Ce_3N@C_{88}$. For cages larger than C_{80}, the cluster-induced strain is weaker than for the C_{80}-I_h cage, whereas cage oxidation potentials are below those for $M_3N@C_{80}$-I_h. Thus, the preference of an endohedral Ce or a fullerene-based oxidation at the first anodic step depends on whether the inner strain is high enough to render a Ce-based oxidation below the oxidation potential of the fullerene cage. It is thus possible that varying the cluster composition can switch the oxidation mechanism.

Titanium and vanadium do not form nitride CFs on their own, but can be incorporated into the nitride CF by a mixed-metal approach. In particular, titan was encapsulated as $TiSc_2N@C_{80}$ and $TiY_2N@C_{80}$, whereas vanadium formed $VSc_2N@C_{80}$ and $V_2ScN@C_{80}$ [96–98]. Comparison of the redox potentials of Ti- and V-containing nitride CFs to those of $Y_3N@C_{80}$ (Table 2.6) shows that their electrochemical properties are largely determined by the transition metals. These

Table 2.6 Redox potentials of selected endohedral metallofullerenes with C_{80}-I_h cage

EMF	Ox-II	Ox-I	Red-I	Red-II	Red-III	Gap_{EC}	References
$Y_3N@C_{80}$-I_h(7)		0.64	−1.41	−1.83		2.05	[84]
$La_2@C_{80}$-I_h(7)	0.95	0.56	−0.31	−1.72	−2.13	0.87	[4]
$Sm_3@C_{80}$-I_h(7)	0.78	0.30	−0.83	−1.88		1.13	[108]
$Sc_3N@C_{80}$-I_h(7)	1.09	0.59	−1.26	−1.62	−2.37	1.85	[69]
$Sc_3CH@C_{80}$-I_h(7)		0.67	−1.21	−1.53	−2.28	1.88	[100]
$Sc_3CN@C_{80}$-I_h(7)		0.60	−1.05	−1.68		1.65	[102]
$Sc_3C_2@C_{80}$-I_h(7)		−0.03	−0.50	−1.64	−1.84	0.47	[109]
$Sc_2TiC@C_{80}$-I_h(7)		0.66	−0.67	−1.51	−1.66	1.33	[106]
$Lu_2TiC@C_{80}$-I_h(7)	1.10	0.63	−0.87	−1.53		1.50	[105]
$Dy_2TiC@C_{80}$-I_h(7)		0.61	−0.97	−1.62	−1.87	1.58	[107]
$Sc_2TiC_2@C_{80}$-I_h(7)		0.53	−0.76	−1.01	−1.96	1.26	[106]
$Dy_2TiC_2@C_{80}$-I_h(7)		0.47	−1.14	−1.58	−2.29	1.61	[107]
$TiSc_2N@C_{80}$-I_h(7)		0.16	−0.94	−1.58		1.10	[99]
$TiY_2N@C_{80}$-I_h(7)		0.00	−1.11	−1.79		1.11	[96]
$VSc_2N@C_{80}$-I_h(7)		0.44	−0.42	−0.66	−1.33	0.86	[98]
$V_2ScN@C_{80}$-I_h(7)		0.60	−0.77	−2.38	–	1.37	[98]
$CeY_2N@C_{80}$-I_h(7)		−0.07	−1.36	−1.88		1.30	[94]
$CeLu_2N@C_{80}$-I_h(7)		0.01	−1.39	−1.88		1.40	[110]
$CeSc_2N@C_{80}$-I_h(7)		0.33	−1.31	−1.83		1.64	[94]
$Sc_4O_2@C_{80}$-I_h(7)	0.79	0.00	−1.10	−1.73		1.10	[101]
$Sc_4C_2@C_{80}$-I_h(7)		0.01	−1.53	−1.97		1.54	[103]
$Sc_4C_2H@C_{80}$-I_h(7)		0.20	−0.87	−1.68	−1.95	1.07	[103]

All values are measured in *o*-dichlorobenzene solution and are referred versus $Fe(Cp)_2^{+/0}$ pair

nitride CFs are paramagnetic and have Ti or V in the formal oxidation state 3+, which is subject to reduction and oxidation within the window of potentials defined by the oxidation and reduction of the fullerene cage. Oxidation of $V_2ScN@C_{80}$ at +0.60 V is the only process which cannot be reliably assigned to the cage or transition metal. Remarkably, Ti- and V-based redox processes in nitride CFs are electrochemically reversible (Fig. 2.11).

Other clusterfullerenes with 6-fold charged cage. For many clusterfullerenes with sixfold charged cluster, C_{80}-I_h cage isomer is the most abundant, or even the only cage isolated in sufficient amounts for electrochemical studies. Comparison of redox potentials of these EMFs to the first oxidation and reduction potentials of $Y_3N@C_{80}$-I_h (Table 2.6) shows that the cluster-based reduction is typical for all of them. All $E_{1/2}(0/-)$ values in Table 2.6 are substantially more positive than −1.41 V reported for $Y_3N@C_{80}$-I_h and span rather broad range, from −1.21 V for $Sc_3CH@C_{80}$ [100] to −0.31 V in the aforementioned $La_2@C_{80}$-I_h [4]. At the same time, the first oxidation potentials for a majority of clusterfullerenes listed in Table 2.6 is close to +0.6 V, which is an indication of the fullerene-based process. Several exception exist though, in which oxidation is also a cluster-based process:

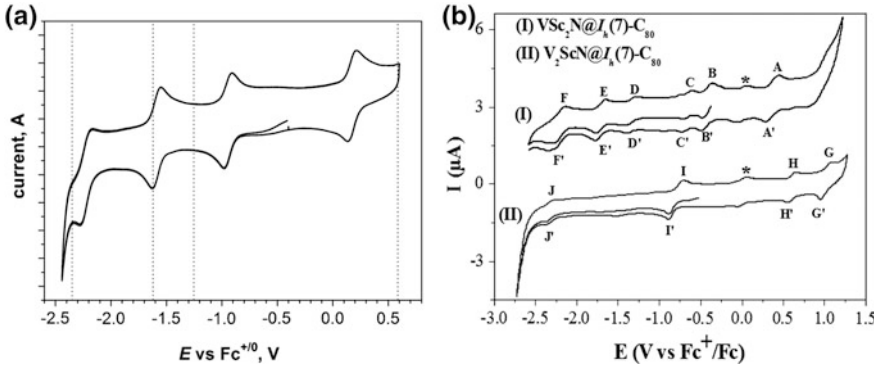

Fig. 2.11 **a** Cyclic voltammogram of Ti-nitride cluster fullerene $TiSc_2N@C_{80}$-I_h(7) (scan rate 20 mV/s, *o*-dichlorobenzene solution), vertical bars denote redox potentials of $Sc_3N@C_{80}$-I_h(7); reproduced with permission from [99]. **b** Cyclic voltammetry of V-nitride clusterfullerenes $VSc_2N@C_{80}$-I_h(7) and $V_2ScN@C_{80}$-I_h(7) (scan rate 100 mV/s, *o*-dichlorobenzene solution); *asterisks* denote redox potential of ferrocene, *block letters* marks redox processes of EMFs. Reproduced with permission from [98]

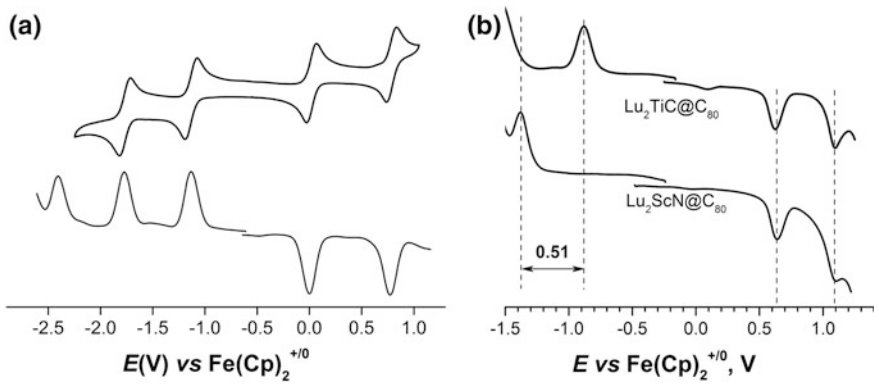

Fig. 2.12 **a** Cyclic voltammetry (*upper trace*) and squarewave voltammetry (*lower trace*) of $Sc_4O_2@C_{80}$-I_h(7) (scan rate 20 mV/s, *o*-dichlorobenzene solution); reproduced with permission from [104]; **b** comparison of the squarewave voltammograms of isoelectronic $Lu_2TiC@C_{80}$-I_h(7) and $Lu_2ScN@C_{80}$-I_h(7) in *o*-dichlorobenzene solution. Note almost identical oxidation potentials and a 0.51 V difference for the reduction potentials

Typical examples are $Sc_4C_2@C_{80}$, $Sc_4O_2@C_{80}$, $M_2TiC_2@C_{80}$ (M = Sc, Dy). Low oxidation potentials are also reported for paramagnetic clusterfullerenes ($Sm_3@C_{80}$, $Sc_3C_2@C_{80}$, or $Sc_4C_2H@C_{80}$), but in this case deviation from a typical values cannot serve as an indication of the cluster-based redox process. Importantly, cluster-based reductions are usually electrochemically reversible.

An overview of the frontier MOs of representative clusterfullerenes with C_{80}-I_h cage, including $La_2@C_{80}$, $Sc_3CN@C_{80}$, $Sc_4C_2@C_{80}$, and $Sc_4O_2@C_{80}$, is given in

Fig. 2.4; frontier MOs of nitride CFs $Sc_3N@C_{80}$-I_h and $Y_3N@C_{80}$-I_h are shown in Fig. 2.8 as discussed above. Spatial localization of the HOMOs and LUMOs in these compounds can again serve as a guide to the experimentally measured redox potentials. For instance, both HOMO and LUMO of $Sc_4O_2@C_{80}$ are predominantly localized on the Sc_4O_2 cluster. Experimentally, $Sc_4O_2@C_{80}$ exhibits reversible reduction and oxidation at 0.00 and −1.10 V (Fig. 2.12), respectively, which is far from the values expected for the fullerene-based redox processes [101]. Indeed, EPR spectroelectrochemistry proved localization of the spin density on the cluster in radical-anion and radical-cation of $Sc_4O_2@C_{80}$ [101]. In $Sc_3CN@C_{80}$, the LUMO is localized on the cluster, and its first reduction potential at −1.05 V is much more positive than the reference cage value of ca −1.4 V. On the contrary, HOMO is largely localized on the cage, and the first oxidation potential of $Sc_3CN@C_{80}$, 0.60 V, is in the range of the values for cage-based oxidation [102]. On the contrary, $Sc_4C_2@C_{80}$ has its HOMO localized on the Sc_4C_2 cluster, and its first oxidation potential is 0.01 V, whereas the LUMO has large cage component, and the first reduction of $Sc_4C_2@C_{80}$ occurs at quite rather negative potential of −1.53 V [103]. Note that in some cases frontier MOs have mixed character with equally considerable contributions from the cluster and the cage (HOMO of $Sc_3NC@C_{80}$, LUMO of $Sc_4C_2@C_{80}$). It can be understood so that the cage and the cluster MOs have equal energies, and hence they are efficiently "hybridized". In such cases, redox potentials of EMFs are usually close to those for EMFs with fullerene-based redox processes.

A special case of *in cavea* electrochemistry is a found in a series of Ti-based carbide CFs with the formulae $M_2TiC@C_{80}$-I_h, where M is Sc, Y, or lanthanides

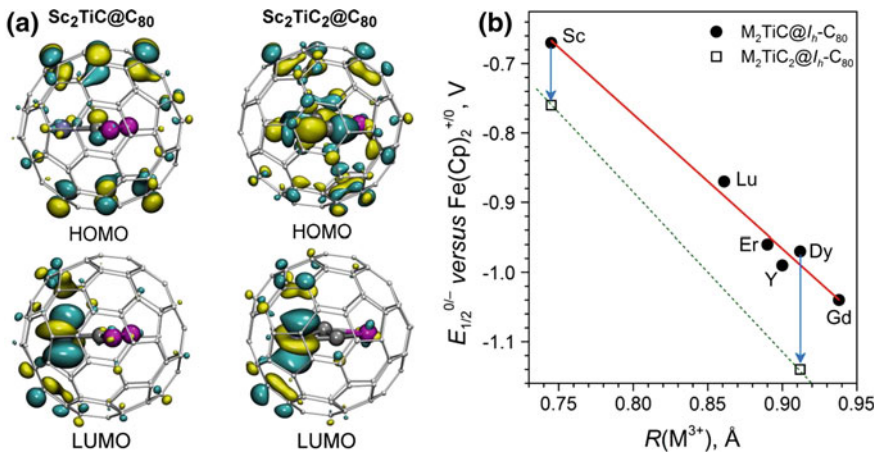

Fig. 2.13 **a** Frontier molecular orbitals of $Sc_2TiC@C_{80}$-I_h(7) and $Sc_2TiC_2@C_{80}$-I_h(7). **b** Dependence of the first reduction potentials in $M_2TiC@C_{80}$-I_h(7) and $M_2TiC_2@C_{80}$-I_h(7) molecules on the ionic radius of M^{3+}. Vertical *blue arrows* mark the shift of the reduction potentials caused by replacement of single central carbon atom by a C_2 unit. Reproduced with permission from [106]

from Gd to Lu [105–107]. $M_2TiC@C_{80}$ carbide CF is isostructural and isoelectronic to $M_2ScN@C_{80}$ nitride CF, and certain similarity in their electronic properties can be expected. Indeed, the HOMO of $M_2TiC@C_{80}$ is essentially a fullerene-based orbital, and hence oxidation potential of all $M_2TiC@C_{80}$ EMFs is close to 0.6 V similar to those of $M_2ScN@C_{80}$ nitride CFs. However, the LUMO of $M_2TiC@C_{80}$ is localized predominantly on the Ti atom (Fig. 2.13a), and the first reduction of $M_2TiC@C_{80}$ EMFs can be thus described as an endohedral Ti^{IV}/Ti^{III}-redox couple with considerably more positive reduction potential than that of $M_2ScN@C_{80}$ (Fig. 2.12b). Interestingly, reduction potentials in the $M_2TiC@C_{80}$ series vary systematically with the ionic radius of M^{3+} (Fig. 2.13b), although these metals are not involved in the electron transfer. The most negative value of −1.04 V is found for $Gd_2TiC@C_{80}$-I_h, whereas the most positive reduction potential of −0.67 V is reported for $Sc_2TiC@C_{80}$-I_h. The reason for such a variation of the Ti^{IV}/Ti^{III}-redox potential in different $M_2TiC@C_{80}$ EMFs is rooted in the inner strain, similar to the situation discussed above for Ce-based nitride CFs. Ionic radius of Ti^{III}, 0.67 Å, is much larger than that of Ti^{IV}, 0.61 Å, and hence the size of the cluster is increased in the reduced state. When the cluster is already rather large (Gd_2TiC), further increase of its size builds up a significant strain caused by the limited inner space in the fullerene cage. Thus, a higher energy (and more negative potential) is needed to add an electron to $Gd_2TiC@C_{80}$ when compared to $Sc_2TiC@C_{80}$ with much smaller cluster. The same reasoning can explain reduction potentials of $M_2TiC_2@C_{80}$. Here LUMO is also Ti-based (Fig. 2.13a), but reduction potentials are more negative than in $M_2TiC@C_{80}$ analogs. Obviously, C_2 unit occupies more space than a single carbon atom, and hence size-driven strain is stronger in $M_2TiC_2@C_{80}$.

2.5 Concluding Remarks

Interaction between metals atoms and clusters with carbon-based π-system in endohedral fullerenes result in fascinating diversity of the electronic structures of EMFs, which also reflects in the electrochemical properties of these molecules. Whereas monometallofullerenes exhibit only fullerene-based redox activity, starting from dimetallofullerenes and to more complex clusters, the frontier orbitals can be partially or completely localized on the endohedral species. As a result, the latter undergo electron transfer reactions independently on the carbon cage. Endohedral electrochemistry thus opens the way to unusual bonding and spin states in charged endohedral metallofullerenes.

References

1. Suzuki T, Maruyama Y, Kato T et al (1993) Electrochemical properties of La@C_{82}. J Am Chem Soc 115(23):11006–11007
2. Suzuki T, Maruyama Y, Kato T et al (1995) Electrochemical properties of fullerenolanthanides. Synth Met 70(1–3):1443–1446
3. Suzuki T, Kikuchi K, Oguri F et al (1996) Electrochemical properties of fullerenolanthanides. Tetrahedron 52(14):4973–4982
4. Suzuki T, Maruyama Y, Kato T et al (1995) Electrochemistry and Ab-Initio study of the dimetallofullerene La_2@C_{80}. Angew Chem-Int Edit Engl 34(10):1094–1096
5. Kikuchi K, Nakao Y, Suzuki S et al (1994) Characterization of the isolated Y@C_{82}. J Am Chem Soc 116(20):9367–9368
6. Xie QS, Perezcordero E, Echegoyen L (1992) Electrochemical detection of C_{60}^{6-} and C_{70}^{6-}—enhanced stability of fullerides in solution. J Am Chem Soc 114(10):3978–3980
7. Reed CA, Bolskar RD (2000) Discrete fulleride anions and fullerenium cations. Chem Rev 100(3):1075–1119
8. Zalibera M, Rapta P, Popov AA et al (2009) Charged states of four isomers of C_{84} fullerene: In Situ ESR and Vis-'NIR Spectroelectrochemistry and DFT Calculations. J Phys Chem C 113(13):5141–5149
9. Zalibera M, Popov AA, Kalbac M et al (2008) The extended view on the empty C_2(3)-C_{82} fullerene: isolation, spectroscopic, electrochemical, and spectroelectrochemical characterization and DFT calculations. Chem-Eur J 14(32):9960–9967
10. Gao XA, Van Caemelbecke E, Kadish KM (1998) Visible and near-infrared absorption spectra of singly and doubly reduced C_{76} fullerene anions. Electrochem Solid State Lett 1 (5):222–223
11. Xie QS, Arias F, Echegoyen L (1993) Electrochemically-reversible, single-electron oxidation of C_{60} and C_{70}. J Am Chem Soc 115(21):9818–9819
12. Dubois D, Kadish KM, Flanagan S et al (1991) Electrochemical detection of fulleronium and highly reduced fulleride C_{60}^{5-} Ions in solution. J Am Chem Soc 113(20):7773–7774
13. Bruno C, Doubitski I, Marcaccio M et al (2003) Electrochemical generation of C_{60}^{2+} and C_{60}^{3+}. J Am Chem Soc 125(51):15738–15739
14. Webster RD, Heath GA (2001) Voltammetric, EPR and UV-VIS-NIR spectroscopic studies associated with the one-electron oxidation of C_{60} and C_{70} in 1,1′,2,2′-tetrachloroethane containing trifluoromethanesulfonic acid. Phys Chem Chem Phys 3(13):2588–2594
15. Yang YF, Arias F, Echegoyen L et al (1995) Reversible fullerene electrochemistry—correlation with the Homo-Lumo energy difference for C_{60}, C_{70}, C_{76}, C_{78}, and C_{84}. J Am Chem Soc 117(29):7801–7804
16. Okada H, Komuro T, Sakai T et al (2012) Preparation of endohedral fullerene containing lithium (Li@C_{60}) and isolation as pure hexafluorophosphate salt ([Li^+@C_{60}][PF_6^-]). RSC Adv 2(28):10624–10631
17. Popov AA, Dunsch L (2011) Electrochemistry in Cavea: endohedral redox reactions of encaged species in fullerenes. J Phys Chem Lett 2(7):786–794
18. Zhang Y, Popov AA (2014) Transition-metal and rare-earth-metal redox couples inside carbon cages: fullerenes acting as innocent ligands. Organometallics 33(18):4537–4549
19. Aoyagi S, Nishibori E, Sawa H et al (2010) A layered ionic crystal of polar Li@C_{60} superatoms. Nat Chem 2(8):678–683
20. Liu J, Shi Z, Gu Z (2009) The cage and metal effect: spectroscopy and electrochemical survey of a series of Sm-containing high metallofullerenes. Chem-Asian J 4(11):1703–1711
21. Lu X, Slanina Z, Akasaka T et al (2010) Yb@C_{2n} (n = 40, 41, 42): new fullerene allotropes with unexplored electrochemical properties. J Am Chem Soc 132(16):5896–5905
22. Xu JX, Li MX, Shi ZJ et al (2005) Electrochemical survey: the effect of the cage size and structure on the electronic structures of a series of ytterbium metallofullerenes. Chem-Eur J 12(2):562–567

23. Zhang Y, Xu JX, Hao C et al (2006) Synthesis, isolation, spectroscopic and electrochemical characterization of some calcium-containing metallofullerenes. Carbon 44(3):475–479
24. Sun BY, Li MX, Luo HX et al (2002) Electrochemical properties of metallofullerenes and their anions. Electrochim Acta 47(21):3545–3549
25. Kuran P, Krause M, Bartl A et al (1998) Preparation, isolation and characterisation of Eu@C_{74}: the first isolated europium endohedral fullerene. Chem Phys Lett 292(4–6):580–586
26. Hu Z, Hao Y, Slanina Z et al (2015) Popular C_{82} fullerene cage encapsulating a divalent metal ion Sm^{2+}: structure and electrochemistry. Inorg Chem 54(5):2103–2108
27. Xu W, Niu B, Feng L et al (2012) Access to an unexplored chiral C_{82} cage by encaging a divalent metal: structural elucidation and electrochemical studies of Sm@C_2(5)-C_{82}. Chem-Eur J 18(45):14246–14249
28. Hao Y, Feng L, Xu W et al (2015) Sm@C_{2v}(19138)-C_{76}: a non-IPR cage stabilized by a divalent metal ion. Inorg Chem 54(9):4243–4248
29. Liu F, Wang S, Guan J et al (2014) Putting a terbium-monometallic cyanide cluster into the C_{82} fullerene cage: TbCN@C_2(5)-C_{82}. Inorg Chem 53(10):5201–5205
30. Yang S, Chen C, Liu F et al (2013) An improbable monometallic cluster entrapped in a popular fullerene cage: YCN@C_s(6)-C_{82}. Sci Rep 3:1487
31. Liu F, Gao C-L, Deng Q et al (2016) Triangular monometallic cyanide cluster entrapped in carbon cage with geometry-dependent molecular magnetism. J Am Chem Soc 138 (44):14764–14771
32. Wang W, Ding J, Yang S et al (1997) Electrochemical properties of 4f-block metallofullerenes. In: Kadish KM, Ruoff RS (eds) Fullerenes. Recent advances in the chemistry and physics of fullerenes and related materials, vol 4. Electrochemical society, Pennington, pp 417–428
33. Yamada M, Feng L, Wakahara T et al (2005) Synthesis and characterization of exohedrally silylated M@C_{82} (M = Y and La). J Phys Chem B 109(13):6049–6051
34. Maeda Y, Matsunaga Y, Wakahara T et al (2004) Isolation and characterization of a carbene derivative of La@C_{82}. J Am Chem Soc 126(22):6858–6859
35. Feng L, Wakahara T, Nakahodo T et al (2006) The bingel monoadducts of La@C_{82}: synthesis, characterization, and electrochemistry. Chem-Eur J 12(21):5578–5586
36. Takano Y, Yomogida A, Nikawa H et al (2008) Radical coupling reaction of paramagnetic endohedral metallofullerene La@C_{82}. J Am Chem Soc 130(48):16224–16230
37. Popov AA, Yang S, Dunsch L (2013) Endohedral fullerenes. Chem Rev 113(8):5989–6113
38. Yamamoto K (1999) Electrochemical study on electronic structure of mono-lanthanofullerenes of La@C_n (n = 82, 86, and 90). In: Kamat PV, Guldi D, Kadish KM (eds) Fullerenes. Recent advances in the chemistry and physics of fullerenes and related materials, vol 7. Electrochemical Society, Pennington, pp 761–770
39. Popov AA, Avdoshenko SM, Pendás AM et al (2012) Bonding between strongly repulsive metal atoms: an oxymoron made real in a confined space of endohedral metallofullerenes. Chem Commun 48:8031–8050
40. Lu X, Nikawa H, Nakahodo T et al (2008) Chemical understanding of a Non-IPR metallofullerene: stabilization of encaged metals on fused-pentagon bonds in La_2@C_{72}. J Am Chem Soc 130:9129–9136
41. Cao BP, Wakahara T, Tsuchiya T et al (2004) Isolation, characterization, and theoretical study of La_2@C_{78}. J Am Chem Soc 126(30):9164–9165
42. Yamada M, Mizorogi N, Tsuchiya T et al (2009) Synthesis and characterization of the D_{5h} isomer of the endohedral dimetallofullerene Ce_2@C_{80}: two-dimensional circulation of encapsulated metal atoms inside a fullerene cage. Chem-Eur J 15:9486–9493
43. Yamada M, Wakahara T, Tsuchiya T et al (2008) Spectroscopic and theoretical study of endohedral dimetallofullerene having a Non-IPR fullerene cage: Ce_2@C_{72}. J Phys Chem A 112:7627–7631
44. Yamada M, Wakahara T, Tsuchiya T et al (2008) Location of the metal atoms in Ce_2@C_{78} and its bis-silylated derivative. Chem Commun 558–560

45. Yamada M, Nakahodo T, Wakahara T et al (2005) Positional control of encapsulated atoms inside a fullerene cage by exohedral addition. J Am Chem Soc 127(42):14570–14571
46. Suzuki M, Mizorogi N, Yang T et al (2013) $La_2@C_s$(17490)-C_{76}: a new non-IPR dimetallic metallofullerene featuring unexpectedly weak metal-pentalene interactions. Chem-Eur J 19 (50):17125–17130
47. Fu W, Zhang J, Fuhrer T et al (2011) $Gd_2@C_{79}N$: isolation, characterization, and monoadduct formation of a very stable heterofullerene with a magnetic spin state of S = 15/2. J Am Chem Soc 133:9741–9750
48. Kato T (2007) Metal dimer and trimer within spherical carbon cage. J Mol Struct 838(1–3):84–88
49. Zuo T, Xu L, Beavers CM et al (2008) $M_2@C_{79}N$ (M = Y, Tb): isolation and characterization of stable endohedral metallofullerenes exhibiting M…M bonding interactions inside Aza[80]fullerene cages. J Am Chem Soc 130(39):12992–12997
50. Kurihara H, Lu X, Iiduka Y et al (2012) $Sc_2@C_{3v}(8)$-C_{82} *vs.* $Sc_2C_2@C_{3v}(8)$-C_{82}: drastic effect of C_2 capture on the redox properties of scandium metallofullerenes. Chem Commun 48:1290–1292
51. Iiduka Y, Wakahara T, Nakajima K et al (2007) Experimental and theoretical studies of the scandium carbide endohedral metallofullerene $Sc_2C_2@C_{82}$ and its carbene derivative. Angew Chem-Int Edit 46(29):5562–5564
52. Tang Q, Abella L, Hao Y et al (2016) $Sc_2O@C_{3v}(8)$-C_{82}: a missing isomer of $Sc_2O@C_{82}$. Inorg Chem 55(4):1926–1933
53. Mercado BQ, Chen N, Rodriguez-Fortea A et al (2011) The shape of the $Sc_2(\mu_2\text{-S})$ unit trapped in C_{82}: crystallographic, computational, and electrochemical studies of the isomers, $Sc_2(\mu_2\text{-S})@C_s(6)$-$C_{82}$ and $Sc_2(\mu_2\text{-S})@C_{3v}(8)$-$C_{82}$. J Am Chem Soc 133(17):6752–6760
54. Zhang M, Hao Y, Li X et al (2014) Facile synthesis of an extensive family of $Sc_2O@C_{2n}$ (n = 35-47) and chemical insight into the smallest member of $Sc_2O@C_2$(7892)-C_{70}. J Phys Chem C 118(49):28883–28889
55. Chen N, Mulet-Gas M, Li Y-Y et al (2013) $Sc_2S@C_2$(7892)-C_{70}: a metallic sulfide cluster inside a non-IPR C_{70} cage. Chem Sci 4(1):180–186
56. Feng Y, Wang T, Wu J et al (2013) Structural and electronic studies of metal carbide clusterfullerene $Sc_2C_2@C_s$-C_{72}. Nanoscale 5(15):6704–6707
57. Chen N, Beavers CM, Mulet-Gas M et al (2012) $Sc_2S@C_s$(10528)-C_{72}: a dimetallic sulfide endohedral fullerene with a Non-IPR cage. J Am Chem Soc 134(18):7851–7860
58. Yang T, Hao Y, Abella L et al (2015) $Sc_2O@T_d$(19151)-C_{76}: hindered cluster motion inside a tetrahedral carbon cage probed by crystallographic and computational studies. Chem-Eur J 21(31):11110–11117
59. Kurihara H, Lu X, Iiduka Y et al (2011) $Sc_2C_2@C_{80}$ rather than $Sc_2@C_{82}$: templated formation of unexpected $C_{2v}(5)$-C_{80} and temperature-dependent dynamic motion of internal Sc_2C_2 cluster. J Am Chem Soc 133(8):2382–2385
60. Tang Q, Abella L, Hao Y et al (2015) $Sc_2O@C_{2v}(5)$-C_{80}: dimetallic oxide cluster inside a C_{80} fullerene cage. Inorg Chem 54(20):9845–9852
61. Samoylova NA, Avdoshenko SM, Krylov DS et al (2017) Confining the spin between two metal atoms within the carbon cage: Redox-active metal-metal bonds in dimetallofullerenes and their stable cation radicals. Nanoscale doi: 10.1039/C7NR02288C
62. Lu X, Nakajima K, Iiduka Y et al (2011) Structural elucidation and regioselective functionalization of an unexplored carbide cluster metallofullerene $Sc_2C_2@C_s(6)$-C_{82}. J Am Chem Soc 133(48):19553–19558
63. Lu X, Nakajima K, Iiduka Y et al (2012) The long-believed $Sc_2@C_{2v}(17)$-C_{84} is actually $Sc_2C_2@C_{2v}(9)$-C_{82}: unambiguous structure assignment and chemical functionalization. Angew Chem-Int Edit Engl 51(24):5889–5892
64. Chen C-H, Ghiassi KB, Cerón MR et al (2015) Beyond the butterfly: $Sc_2C_2@C_{2v}(9)$-C_{86}, an endohedral fullerene containing a planar, twisted Sc_2C_2 unit with remarkable crystalline order in an unprecedented carbon cage. J Am Chem Soc 137(32):10116–10119

65. Popov AA, Dunsch L (2008) Hindered cluster rotation and ^{45}Sc hyperfine splitting constant in distonoid anion radical $Sc_3N@C_{80}$, and spatial spin charge separation as a general principle for anions of endohedral fullerenes with metal-localized lowest unoccupied molecular orbitals. J Am Chem Soc 130(52):17726–17742
66. Jakes P, Dinse KP (2001) Chemically induced spin transfer to an encased molecular cluster: an EPR study of $Sc_3N@C_{80}$ radical anions. J Am Chem Soc 123(36):8854–8855
67. Yang SF, Zalibera M, Rapta P et al (2006) Charge-induced reversible rearrangement of endohedral fullerenes: electrochemistry of tridysprosium nitride clusterfullerenes $Dy_3N@C_{2n}$ (2n = 78, 80). Chem-Eur J 12(30):7848–7855
68. Tarabek J, Yang S, Dunsch L (2009) Redox properties of mixed lutetium/yttrium nitride clusterfullerenes: endohedral $Lu_xY_{3-x}N@C_{80}$(I) (x = 0-3) compounds. Chem Phys Chem 10 (7):1037–1043
69. Elliott B, Yu L, Echegoyen L (2005) A simple isomeric separation of D_{5h} and I_h $Sc_3N@C_{80}$ by selective chemical oxidation. J Am Chem Soc 127(31):10885–10888
70. Chaur MN, Athans AJ, Echegoyen L (2008) Metallic nitride endohedral fullerenes: synthesis and electrochemical properties. Tetrahedron 64(50):11387–11393
71. Rapta P, Popov AA, Yang SF et al (2008) The charged states of $Sc_3N@C_{68}$: an in situ spectroelectrochemical study of the radical cation and radical anion of a Non-IPR fullerene. J Phys Chem A 112:5858–5865
72. Popov AA, Avdoshenko SM, Cuniberti G et al (2011) Dimerization of radical-anions: nitride clusterfullerenes versus empty fullerenes. J Phys Chem Lett 1592–1600
73. Konarev DV, Zorina LV, Khasanov SS et al (2016) A crystalline anionic complex of scandium nitride endometallofullerene: experimental observation of single-bonded $(Sc_3N@I_h\text{-}C_{80}^-)_2$ dimers. Chem Commun 52:10763–10766
74. Yang SF, Rapta P, Dunsch L (2007) The spin state of a charged non-IPR fullerene: the stable radical cation of $Sc_3N@C_{68}$. Chem Commun 2:189–191
75. Chaur MN, Aparicio-Angles X, Mercado BQ et al (2010) Structural and electrochemical property correlations of metallic nitride endohedral metallofullerenes. J Phys Chem C 114 (30):13003–13009
76. Cai T, Xu LS, Anderson MR et al (2006) Structure and enhanced reactivity rates of the D_{5h} $Sc_3N@C_{80}$ and $Lu_3N@C_{80}$ metallofullerene isomers: the importance of the pyracylene motif. J Am Chem Soc 128(26):8581–8589
77. Wei T, Wang S, Liu F et al (2015) Capturing the long-sought small-bandgap endohedral fullerene $Sc_3N@C_{82}$ with low kinetic stability. J Am Chem Soc 137(8):3119–3123
78. Beavers CM, Chaur MN, Olmstead MM et al (2009) Large metal ions in a relatively small fullerene cage: the structure of $Gd_3N@C_2$(22010)-C_{78} departs from the isolated pentagon rule. J Am Chem Soc 131(32):11519–11524
79. Chaur MN, Melin F, Elliott B et al (2007) $Gd_3N@C_{2n}$ (n = 40, 42, and 44): remarkably low HOMO-LUMO gap and unusual electrochemical reversibility of $Gd_3N@C_{88}$. J Am Chem Soc 129(47):14826–14829
80. Fu W, Zhang J, Champion H et al (2011) Electronic properties and ^{13}C NMR structural study of $Y_3N@C_{88}$. Inorg Chem 50(10):4256–4259
81. Chaur MN, Melin F, Elliott B et al (2008) New $M_3N@C_{2n}$ endohedral metallofullerene families (M = Nd, Pr, Ce; n = 40-53): expanding the preferential templating of the C_{88} cage and approaching the C_{96} cage. Chem-Eur J 14(15):4594–4599
82. Chaur MN, Valencia R, Rodriguez-Fortea A et al (2009) Trimetallic nitride endohedral fullerenes: experimental and theoretical evidence for the $M_3N^{6+}@C_{2n}^{6-}$ model. Angew Chem-Int Edit 48(8):1425–1428
83. Chaur MN, Melin F, Ashby J et al (2008) Lanthanum nitride endohedral fullerenes $La_3N@C_{2n}$ (43 < n < 55): preferential formation of $La_3N@C_{96}$. Chem-Eur J 14(27):8213–8219
84. Cardona CM, Elliott B, Echegoyen L (2006) Unexpected chemical and electrochemical properties of $M_3N@C_{80}$ (M = Sc, Y, Er). J Am Chem Soc 128(19):6480–6485

85. Li F-F, Pinzon JR, Mercado BQ et al (2011) [2 + 2] cycloaddition reaction to $Sc_3N@I_h$-C_{80}. The formation of very stable [5,6]- and [6,6]-adducts. J Am Chem Soc 133(5):1563–1571
86. Pinzon JR, Zuo TM, Echegoyen L (2010) Synthesis and electrochemical studies of bingel-hirsch derivatives of $M_3N@I_h$-C_{80} (M = Sc, Lu). Chem-Eur J 16(16):4864–4869
87. Li F-F, Rodríguez-Fortea A, Peng P et al (2012) Electrosynthesis of a $Sc_3N@I_h$-C_{80} methano derivative from trianionic $Sc_3N@I_h$-C_{80}. J Am Chem Soc 134(17):7480–7487
88. Feng L, Gayathri Radhakrishnan S, Mizorogi N et al (2011) Synthesis and charge-transfer chemistry of $La_2@I_h$-C_{80}/$Sc_3N@I_h$-C_{80}-Zinc porphyrin conjugates: impact of endohedral cluster. J Am Chem Soc 133(19):7608–7618
89. Wakahara T, Iiduka Y, Ikenaga O et al (2006) Characterization of the bis-silylated endofullerene $Sc_3N@C_{80}$. J Am Chem Soc 128(30):9919–9925
90. Popov AA, Shustova NB, Svitova AL et al (2010) Redox-tuning endohedral fullerene spin states: from the dication to the trianion radical of $Sc_3N@C_{80}(CF_3)_2$ in five reversible single-electron steps. Chem-Eur J 16(16):4721–4724
91. Shustova NB, Peryshkov DV, Kuvychko IV et al (2011) Poly(perfluoroalkylation) of metallic nitride fullerenes reveals addition-pattern guidelines: synthesis and characterization of a family of $Sc_3N@C_{80}(CF_3)_n$ (n = 2-16) and their radical anions. J Am Chem Soc 133 (8):2672–2690
92. Piro NA, Robinson JR, Schelter EJ (2014) The electrochemical behavior of cerium(III/IV) complexes: thermodynamics, kinetics and applications in synthesis. Coord Chem Rev 260:21–36
93. Vargová A, Popov A, Rapta P et al (2010) Electrochemical tuning of spin states of the endohedral metallofullerene $Y@C_{82}$ as probed by ESR spectroelectrochemistry. Chem Phys Chem 11(8):1650–1653
94. Zhang Y, Schiemenz S, Popov AA et al (2013) Strain-driven endohedral redox couple Ce^{IV}/Ce^{III} in nitride clusterfullerenes $CeM_2N@C_{80}$ (M = Sc, Y, Lu). J Phys Chem Lett 4:2404–2409
95. Zhang Y, Popov AA, Dunsch L (2014) Endohedral metal or a fullerene cage based oxidation? Redox duality of nitride clusterfullerenes $Ce_xM_{3-x}N@C_{78-88}$ (x = 1, 2; M = Sc and Y) dictated by the encaged metals and the carbon cage size. Nanoscale 6:1038–1048
96. Chen C, Liu F, Li S et al (2012) Titanium/yttrium mixed metal nitride clusterfullerene $TiY_2N@C_{80}$: synthesis, isolation, and effect of the group-III metal. Inorg Chem 51(5):3039–3045
97. Yang S, Chen C, Popov A et al (2009) An endohedral titanium(III) in a clusterfullerene: putting a non-group-III metal nitride into the C_{80}-I_h fullerene cage. Chem Commun 6391–6393
98. Wei T, Wang S, Lu X et al (2016) Entrapping a group-VB transition metal, vanadium, within an endohedral metallofullerene: $V_xSc_{3-x}N@I_h$-C_{80} (x = 1, 2). J Am Chem Soc 138 (1):207–214
99. Popov AA, Chen C, Yang S et al (2010) Spin-flow vibrational spectroscopy of molecules with flexible spin density: electrochemistry, ESR, cluster and spin dynamics, and bonding in $TiSc_2N@C_{80}$. ACS Nano 4(8):4857–4871
100. Junghans K, Rosenkranz M, Popov AA (2016) $Sc_3CH@C_{80}$: selective ^{13}C enrichment of the central carbon atom. Chem Commun 52:6561–6564
101. Popov AA, Chen N, Pinzón JR et al (2012) Redox-active scandium oxide cluster inside a fullerene cage: spectroscopic, voltammetric, electron spin resonance spectroelectrochemical, and extended density functional theory study of $Sc_4O_2@C_{80}$ and its ion radicals. J Am Chem Soc 134(48):19607–19618
102. Wang T-S, Feng L, Wu J-Y et al (2010) Planar quinary cluster inside a fullerene cage: synthesis and structural characterizations of $Sc_3NC@C_{80}$-I_h. J Am Chem Soc 132 (46):16362–16364
103. Feng Y, Wang T, Wu J et al (2014) Electron-spin excitation by implanting hydrogen into metallofullerene: the synthesis and spectroscopic characterization of $Sc_4C_2H@I_h$-C_{80}. Chem Commun 50(81):12166–12168

104. Elliott B, Pykhova AD, Rivera J et al (2013) Spin density and cluster dynamics in $Sc_3N@C_{80}^-$ upon [5,6] exohedral functionalization: an ESR and DFT study. J Phys Chem C 117(5):2344–2348
105. Svitova AL, Ghiassi K, Schlesier C et al (2014) Endohedral fullerene with μ_3-carbido ligand and titanium-carbon double bond stabilized inside a carbon cage. Nat Commun 5:3568. doi:3510.1038/ncomms4568
106. Junghans K, Ghiassi KB, Samoylova NA et al (2016) Synthesis and isolation of the titanium-scandium endohedral fullerenes—$Sc_2TiC@I_h$-C_{80}, $Sc_2TiC@D_{5h}$-C_{80}, and $Sc_2TiC_2@I_h$-C_{80}: metal size tuning of the Ti^{IV}/Ti^{III} redox potentials. Chem-Eur J 22 (37):13098–13107
107. Junghans K, Schlesier C, Kostanyan A et al (2015) Methane as a selectivity booster in the arc-discharge synthesis of endohedral fullerenes: selective synthesis of the single-molecule magnet $Dy_2TiC@C_{80}$ and its congener $Dy_2TiC_2@C_{80}$. Angew Chem-Int Edit Engl 54 (45):13411–13415
108. Xu W, Feng L, Calvaresi M et al (2013) An experimentally observed trimetallofullerene $Sm_3@I_h$-C_{80}: encapsulation of three metal atoms in a cage without a nonmetallic mediator. J Am Chem Soc 135(11):4187–4190
109. Wakahara T, Sakuraba A, Iiduka Y et al (2004) Chemical reactivity and redox property of $Sc_3@C_{82}$. Chem Phys Lett 398:553–556
110. Zhang L, Popov AA, Yang S et al (2010) An endohedral redox system in a fullerene cage: the Ce based mixed cluster fullerene $Lu_2CeN@C_{80}$. Phys Chem Chem Phys 12:7840–7847

http://www.springer.com/978-3-319-47047-4

Endohedral Fullerenes: Electron Transfer and Spin
Popov, A. (Ed.)
2017, XII, 328 p. 167 illus., 84 illus. in color., Hardcover
ISBN: 978-3-319-47047-4